Plant-Necrotroph Co-transcriptome Networks Illuminate a Metabolic Battlefield

Wei Zhang[1,2], Jason A. Corwin[3], Daniel Copeland[2], Julie Feusier[2], Robert Eshbaugh[2], David E. Cook[1], Susana Atwell[2], and Daniel J. Kliebenstein[2,4*]

[1]Department of Plant Pathology, Kansas State University, 1712 Clafflin Road, Throckmorton Hall, Manhattan, KS, 66506, USA

[2]Department of Plant Sciences, University of California, Davis, One Shields Avenue, Davis, CA, 95616, USA

[3]Department of Ecology and Evolution Biology, University of Colorado, 1900 Pleasant Street, 334 UCB, Boulder, CO, 80309-0334, USA

[4]DynaMo Center of Excellence, University of Copenhagen, Thorvaldsensvej 40, DK-1871, Frederiksberg C, Denmark

***Correspondence:** Daniel J. Kliebenstein, Department of Plant Sciences, University of California, Davis, One Shields Ave, Davis, CA, 95616, USA.

kliebenstein@ucdavis.edu

Phone: 530-754-7775

Running title: Co-transcriptome Networks between Arabidopsis and *Botrytis cinerea*

Keywords: Host-pathogen Interaction, Co-transcriptome, Gene Co-expression Network, Pathosystem, Arabidopsis, *Botrytis cinerea*

Abstract

A central goal of studying host-pathogen interaction is to understand how host and pathogen manipulate each other to promote their own fitness in a pathosystem. Co-transcriptomic approaches can simultaneously analyze dual transcriptomes during infection and provide a systematic map of the cross-kingdom communication between two species. Here we used the Arabidopsis-*B. cinerea* pathosystem to test how plant host and fungal pathogen interact at the transcriptomic level. We assessed the impact of genetic diversity in pathogen and host by utilization of a collection of 96 isolates infection on Arabidopsis wild-type and two mutants with jasmonate or salicylic acid compromised immunities. We identified ten *B. cinerea* gene co-expression networks (GCNs) that encode known or novel virulence mechanisms. Construction of a dual interaction network by combining four host- and ten pathogen-GCNsrevealed potential connections between the fungal and plant GCNs. These co-transcriptome data shed lights on the potential mechanisms underlying host-pathogen interaction.

41 **INTRODUCTION**

42 How a host and pathogen manipulate each other within a pathosystem to facilitate their own
43 fitness remains a long-standing question. The difference between the pathogen's ability to infect
44 and the host's ability to resist generates the resulting disease symptomology. This interaction
45 forces host-pathogen dynamics to shape the genomes of the two species via adaptive responses to
46 each other (Dangl and Jones, 2001; Bergelson et al., 2001; Benton, 2009; Kanzaki et al., 2012;
47 Karasov et al., 2014). Plants have evolved a sophisticated set of constitutive and inducible
48 immune responses to cope with constant selective pressures from antagonistic microbes (Jones
49 and Dangl, 2006). Reciprocally, plant pathogens have also evolved a variety of different invasion
50 and virulence strategies to disarm or circumvent plant defense strategies (Glazebrook, 2005;
51 Toruno et al., 2016). This has resulted in complex relations between plant hosts and fungal
52 pathogens for survival and fitness.

53 The plant innate immune system includes several functional layers with overlapping functions to
54 detect and defend against phytopathogens. This multi-layer immune system can be categorized
55 as a signal monitor system to detect invasion, local and systemic signal transduction components
56 to elicit and coordinate responses, and defensive response proteins and metabolites focused on
57 combatting the invading pathogen (Tsuda and Katagiri, 2010; Corwin and Kliebenstein, 2017).
58 These functional layers, as well as the components within them, are highly interconnected and
59 tightly regulated by the host plant to respond appropriately to various phytopathogens (Couto
60 and Zipfel, 2016; Tang et al., 2017). For instance, Arabidopsis utilizes a complex signaling
61 network to regulate the production of indole-derived secondary metabolites, such as camalexin
62 and indole glucosinolates, that contribute to resistance against pathogens (Kliebenstein et al.,
63 2005; Clay et al., 2009; Bednarek et al., 2009; Frerigmann et al., 2016; Xu, J. et al., 2016;

64 Mine et al., 2018). This layered immune system provides pathogens with numerous targets in the
65 plant immune system that the pathogen can utilize, evade or attack. Most biotrophic pathogens,
66 evolved from commensal microbes, attempt to dismantle the plant immune system by injecting
67 effector proteins into host cells or the inter-cellular space (Dangl and Jones, 2001; Buttner and
68 He, 2009; Stergiopoulos and de Wit, 2009). For example, the biotrophic bacterial pathogen
69 *Pseudomonas syringae* can utilize the jasmonic acid (JA) signaling pathway through the
70 production of a JA-mimic, coronatine, to enhance its fitness (Mittal and Davis, 1995; Brooks et
71 al., 2005; Cui et al., 2018). Alternatively, necrotrophic pathogens, which often evolved from
72 environmental saprophytic microbes, can utilize toxic secondary metabolites, small secreted
73 proteins, and small RNAs to aggressively attack host defenses while also defending against host-
74 derived toxins (Choquer et al., 2007; Arbelet et al., 2010; Mengiste, 2012; Weiberg et al.,
75 2013; Kubicek et al., 2014; Macheleidt et al., 2016). In addition, pathogens can directly resist
76 downstream defenses as is done by *B. cinerea*, where it has an ATP-binding cassette (ABC)
77 transporter BcatrB that provides resistance by exporting camalexin from the pathogen cell
78 (Stefanato et al., 2009). This high level of interactivity between the immune system and
79 pathogen virulence mechanisms generates the final level of disease severity. However, a
80 functional description of this combative cross-kingdom communication between a plant host and
81 necrotrophic pathogen remains elusive.

82 Co-transcriptomic approaches whereby the host and pathogen transcriptomes are simultaneously
83 analyzed provide the ability to systematically map the cross-kingdom communication between
84 plant hosts and their pathogens, both for individual genes and gene co-expression network
85 (GCN) levels (Stuart et al., 2003; Musungu et al., 2016; Zhang, W. et al., 2017; Lanver et al.,
86 2018; McClure et al., 2018). Recent advances have enabled the measurement of pathogen *in*

87 *planta* transcriptome. For example, *in planta* measurements of the pathogens' transcriptome
88 within the biotrophic Arabidopsis-*Pseudomonas syringae* pathosystem has enabled the
89 investigation of early effects on Arabidopsis host immunity and the consequent effects on
90 bacterial growth (Nobori et al., 2018). This enabled the identification of a bacterial iron
91 acquisition pathway that is suppressed by multiple plant immune pathways (Nobori et al., 2018).
92 This shows the potential for new hypothesis to be generated by a co-transcriptome approach
93 (Swierzy et al., 2017; Westermann et al., 2017; Lee et al., 2018).

94 The Arabidopsis-*B. cinerea* pathosystem is well suited for exploring plant-pathogen interaction
95 to understand host defenses and necrotrophic virulence in ecological and agricultural settings. *B.*
96 *cinerea* is a necrotrophic generalist pathogen that attacks a broad range of diverse plant hosts,
97 including dicots, gymnosperms, and even bryophytes (Williamson et al., 2007). This
98 necrotrophic pathogen is endemic throughout the world and can cause severe pre- and post-
99 harvest losses in many crops. A high level of standing natural genetic variation within *B. cinerea*
100 population is hypothesized to facilitate the extreme host range of *B. cinerea*. This genetic
101 variation affects nearly all known *B. cinerea* virulence strategies, including penetration and
102 establishment, evading detection, and combatting/coping with plant immune responses (Atwell
103 et al., 2015; Walker et al., 2015; Corwin, Subedy et al., 2016). For example, a key virulence
104 mechanism is the secretion of phytotoxic secondary metabolites, including the sesquiterpene
105 botrydial (BOT) and the polyketide botcinic acid (BOA) that trigger plant chlorosis and host cell
106 collapse (Deighton et al., 2001; Colmenares et al., 2002; Wang et al., 2009; Rossi et al., 2011;
107 Ascari et al., 2013; Porquier, A. et al., 2016). These metabolites are linked to virulence, but
108 some pathogenic field isolates fail to produce either compounds pointing to additional
109 pathogenic strategies. The combination of a high level of genetic diversity and extensive

110 recombination means that a population of *B. cinerea* is a mixed collection of virulence strategies
111 that can be used to interrogate by the co-transcriptome.

112 In the present study, we used the Arabidopsis-*B. cinerea* pathosystem to test how the
113 transcriptomes of the two species interact during infection and assess how natural genetic
114 variation in the pathogen impacts disease development. Isolates were inoculated on Arabidopsis
115 Col-0 wild-type (WT) in conjunction with immune-deficient hormone mutants *coi1-1* (jasmonate
116 defense signaling) and *npr1-1* (salicylic acid defense signaling). For the pathogen, we utilized a
117 collection of 96 isolates of *B. cinerea* that harbor a wide scope of natural genetic variation within
118 the species (Atwell et al., 2015; Corwin et al., 2016; Zhang et al., 2016; Corwin, Copeland et
119 al., 2016; Zhang et al., 2017; Soltis et al., 2018; Fordyce et al., 2018). From individual
120 infected leaves, we simultaneously measured both the Arabidopsis and *B. cinerea* transcripts at
121 16 hours post-infection (HPI). We have previously analyzed the Arabidopsis transcripts to
122 identify four host-derived GCNs that are sensitive to natural genetic variation in *B. cinerea*
123 (Zhang et al., 2017). In present analysis, we identified ten fungal pathogen-derived GCNs that
124 encode either known or novel virulence mechanisms within the species. Some of these *B. cinerea*
125 GCNs responsible for BOT production, exocytosis regulation and copper transport are highly
126 linked with the host's defense phytohormone pathways. By combining the plant host- and
127 pathogen-GCNs into a single network, we constructed a dual-transcriptomic network that
128 identifies potential interactions between the components of plant host innate immune system and
129 fungal pathogen virulence. These connections highlight potential targets for fungal pathogen
130 phytotoxins and prevailing counter-responses from plant host. Collectively, co-transcriptomic
131 analysis shed lights on the potential mechanisms underlying how the host and pathogen combat

132 each other during infection and illustrate the continued need for advancements of *in planta*
133 analysis of dual-species interaction.

134 **RESULTS**

135 **Genetic Variation in Pathogen and Hosts Influence *B. cinerea* Transcriptome**

136 To investigate how genetic variation within a pathogen differentially interacts with plant host
137 immunity at the transcriptomic level, we profiled the *in planta* transcriptomes of 96 *B. cinerea*
138 isolates infection across three host genotypes, the Arabidopsis accession Col-0 WT and two
139 immune-signaling mutants *coi1-1* and *npr1-1* that are respectively compromised in JA or
140 salicylic acid (SA) driven immunity. This previously described collection of 96 isolates
141 represents a broad geographical distribution and contains considerable natural genetic variation
142 that affects a diversity of virulence strategies within *B. cinerea* (Denby et al., 2004; Rowe and
143 Kliebenstein, 2007; Atwell et al., 2015; Corwin et al., 2016; Zhang et al., 2016). Four
144 independent biological replicates across two separate experiments per isolate/genotype pair were
145 harvested at 16HPI for transcriptome analysis. A total of 1,152 independent RNA samples were
146 generated for library preparation and sequenced on Illumina HiSeq platform (NCBI accession
147 number SRP149815). These libraries were previously used to study Arabidopsis transcriptional
148 responses to natural genetic variation in *B. cinerea* (Zhang et al., 2017). Mapping the dual-
149 transcriptome reads against the *B. cinerea* reference genome (B05.10), we identified 9,284
150 predicted gene models with a minimum of either 30 gene counts in one isolate or 300 gene
151 counts across 96 isolates. The total of identified genes corresponds to ~79% of the 11,701
152 predicted encoding genes in B05.10 reference genome (Supplemental Data Set 1 to 3) (Van Kan

153 et al., 2017). The two different thresholds allowed the identification of pathogen transcripts that
154 express only in a specific isolate.

155 Measuring the abundance of individual pathogen transcripts in relation to the host transcripts can
156 be used as a molecular method to estimate fungal biomass (Blanco-Ulate et al., 2014). Given
157 this, we hypothesized that the fraction of total reads that map to *B. cinerea* might be a
158 biologically relevant indicator of pathogen virulence (Supplemental Data Set 4). Comparing *B.*
159 *cinerea* transcript abundance at 16HPI to lesion development at 72HPI revealed a significant
160 partial correlation in the WT Col-0 (R^2 = 0.1101, *P*-value = 0.0016, Figure 1). In contrast to WT,
161 the early transcriptomic activities of most *B. cinerea* isolates were more vigorous in the two
162 Arabidopsis mutants, resulting in a significant curvilinear relationship between total fraction of
163 *B. cinerea* reads and final lesion area (*P*-value = 3.914e-07, *P*-value = 0.0001, respectively,
164 Figure 1). Interestingly, the total reads fraction was better correlated with final lesion area in
165 *coi1-1* (R^2= 0.2562) than either WT (R^2 = 0.1101) or *npr1-1* (R^2 = 0.161). This suggests that
166 early transcriptomic activity from the pathogen can be a partial indicator of pathogen virulence,
167 but also depends on the respective resistance from the plant host.

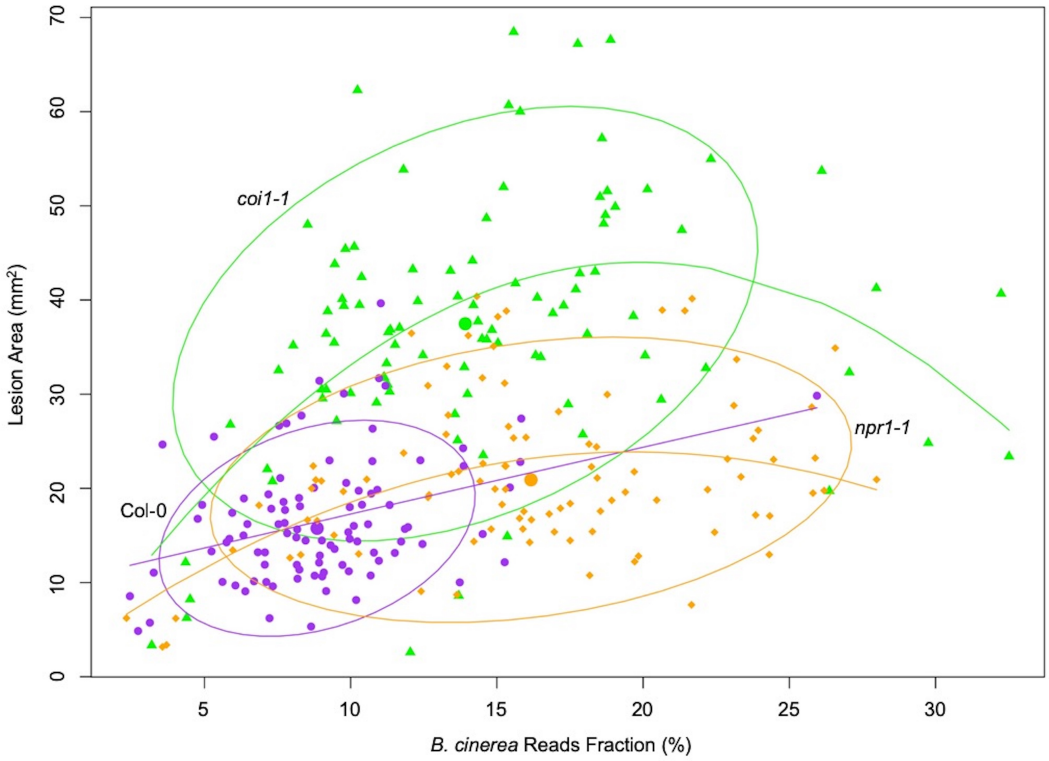

Figure 1. Correlation between earlier estimated *B. cinerea* biomass and later lesion area. Model-corrected lesion area means were estimated using the linear model on the six replicates data from three Arabidopsis genotypes at 72-hours post-infection with 96 *B. cinerea* isolates. Estimated biomass of *B. cinerea* was calculated using the linear model-corrected fraction of *B. cinerea* mapped reads against total mapped reads to Arabidopsis and *B. cinerea* reference genomes. RNA-Seq analysis was conducted at 16-hours post-infection for each pathosystem. Three Arabidopsis genotypes are wild-type Col-0 (purple dot), jasmonate insensitive mutant *coi1-1* (green triangle), and salicylic acid insensitive mutant *npr1-1* (orange diamond). The 90% confidence ellipse intervals are plotted for each Arabidopsis genotype for references. Quadratic regression lines are: Col-0: $y = -0.00059x^2 + 0.729x + 10.037$, $P = 0.0016$, adjusted $R^2 = 0.1101$; *coi1-1*: $y = -0.117x^2 + 4.44x - 0.1585$, $P = 3.914e\text{-}07$, adjusted $R^2 = 0.2562$; *npr1-1*: $y = -0.0579x^2 + 2.26x + 1.673$, $P = 0.0001$, adjusted $R^2 = 0.161$.

Plant defense phytohormone networks, like SA and JA, help shape the immune responses of a plant host while also shape the virulence gene expression within bacterial pathogens, such as *Pseudomonas syringae* (Nobori et al., 2018). To test how variation in host SA/JA-signaling influences the fungal pathogen transcriptome, we applied a generalized linear model linked with negative-binomial function (nbGLM) to each *B. cinerea* transcript across the experiment. This analysis allowed us to estimate the relative broad-sense heritability (H^2) of genetic variation from the pathogen, plant host, or their interaction contributing to each transcript. Of the 9,284 detectable *B. cinerea* transcripts, 8,603 and 5,244 transcripts were significantly influenced by

177 genetic variation in pathogen and host, respectively (74% and 45% of predicted *B. cinerea* gene
178 models, respectively) (Figure 2A, Supplemental Data Set 3 and 5). While this result shows that
179 the plant phytohormone pathways influence *B. cinerea* gene expression, the variation in host
180 defense responses (average $H^2_{\text{Host}} = 0.010$) has far less influence on *B. cinerea* gene expression
181 than that of the pathogens' own natural genetic variation (average $H^2_{\text{Isolate}} = 0.152$). The host
182 defense hormones also affected *B. cinerea* gene expression in a genotype-by-genotype dependent
183 manner on 4,541 genes (39% of *B. cinerea* predicted gene models, average $H^2_{\text{Isolate x Host}} = 0.116$)
184 (Figure 2B-2I). Illustrating this potential for host x pathogen interactions on pathogen gene
185 expression are the two genes encoding the well-studied polygalacturonase 1 (*Bcpg1*) and
186 oxaloacetate acetyl hydrolase. *Bcpg1* has dramatic expression variation across 96 isolates in
187 different host backgrounds (Figure 3, Figure 3-figure supplemental 1, and Supplemental Data Set
188 1). Extending this to 500 genes showing the strongest host x pathogen effect showed that there is
189 a wide range of patterns that differs in the host *coi1-1* or *npr1-1* background with diverse
190 pathogen strain specific patterns (Figure 4). One potential complication of this analysis is for
191 sequence variation between the reference B05.10 genome and the diverse strains to create
192 artificially low expression estimates. However, very few genes showed consistently low
193 expression within a strain and instead when a gene showed no expression in one host genotype, it
194 was expressed in a different host genotype (Figure 3 and supplemental Table 1). This
195 conditionality argues against a sequencing error as the sequence has not altered. The genes that
196 did show a loss of expression across all host genotypes within a strain (i.e. BOT and BOA genes)
197 were frequently linked to whole gene deletions that abolished their expression (Soltis et al.,
198 2019). Thus, while there are likely some sequence variation associated expression errors, they are
199 not a dominant signature in the data. Thus, within the Arabidopsis/*B. cinerea* pathosystem the

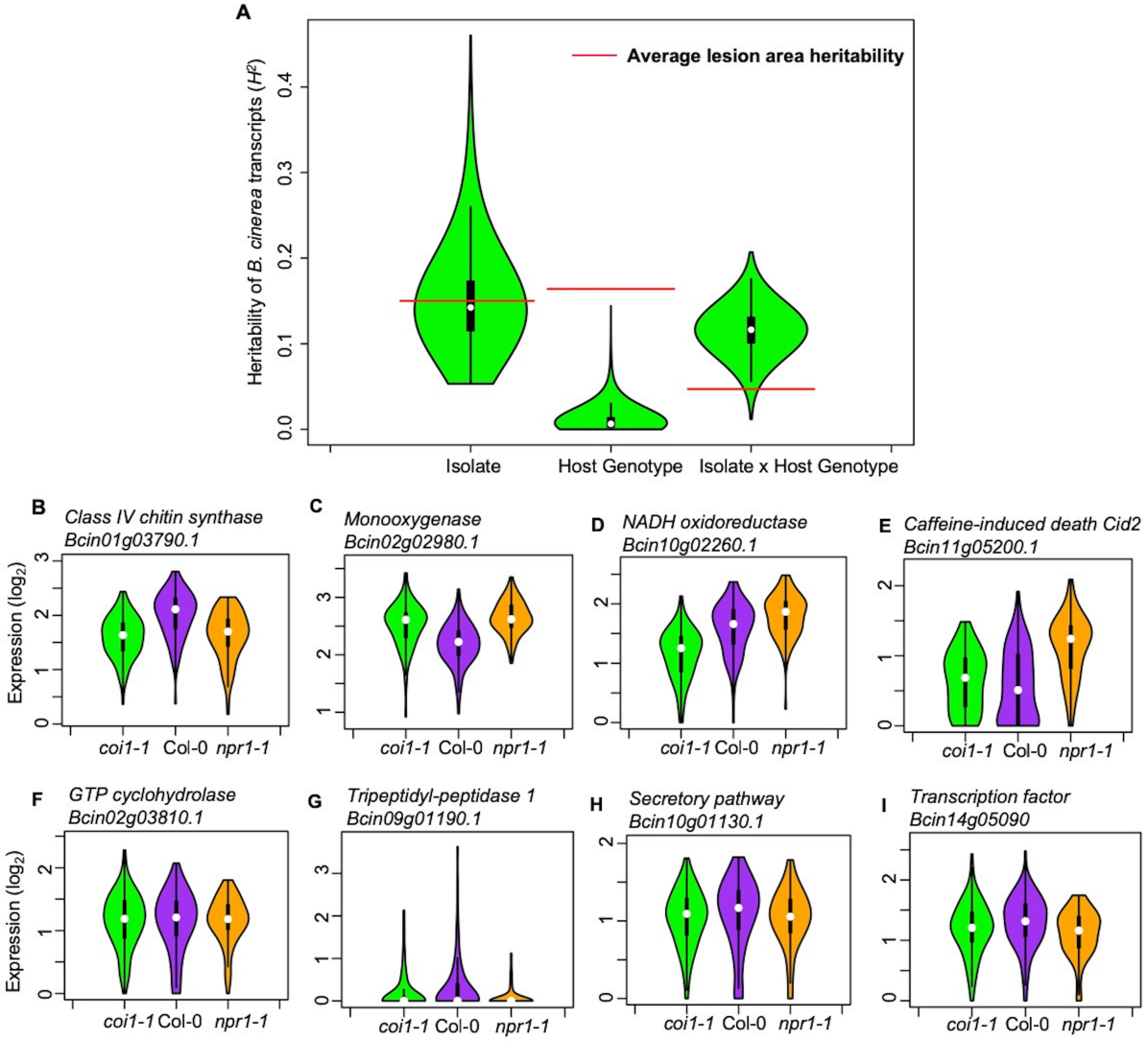

Figure 2. Transcriptomic responses of *B. cinerea* on Arabidopsis are controlled by genetic variation in pathogen population, host genotypes, and their interaction. (A) Distribution of broad-sense heritability (H^2) of *B. cinerea* transcripts contributed by genetic variation in the *B. cinerea*, Arabidopsis genotypes, and the interaction between pathogen and host. Violin plots illustrating the distribution of H^2 for transcripts from 96 *B. cinerea* isolates infecting on Arabidopsis genotypes. Heritability is partitioned across the different sources, 96 pathogen genotypes = "Isolate", plant genotypes Col-0, *coi1-1* and *npr1-1* plant genotypes = "Host", and the corresponding interaction. The transcriptomic analysis was conducted by sequencing mRNA extracted from *B. cinerea* infected Arabidopsis leaves at 16-hours post-infection. Red lines indicate the average broad-sense heritability values of lesion area caused by isolates, Arabidopsis genotypes, and their interaction. (B) to (E) Expression profiles of *B. cinerea* transcripts significantly influenced by host genotypes. The model-corrected means ($\log_2$) for *B. cinerea* transcript were used for plotting. The Arabidopsis genotypes, wild-type Col-0 (purple), jasmonate insensitive mutant *coi1-1* (green), and salicylic acid mutant *npr1-1* (orange), are shown on the x axis. *B. cinerea* transcripts are: (B) *Bcin01g03790.1*, class IV chitin synthase; (C) *Bcin02g02980.1*, Monooxygenase; (D) *Bcin10g02260.1*, NADH oxidoreductase; (E) *Bcin11g05200.1*, caffeine-induced death Cid2; (F) to (I) Expression profiles of *B. cinerea* transcripts significantly influenced by the interaction between pathogen and host genotypes. (F) *Bcin02g03810.1*, GTP cyclohydrolase; (G) *Bcin09g01190.1*, Tripeptidyl-peptidase 1; (H) *Bcin10g01130.1*, in secretory pathway; (I) *Bcin14g05090.1*, a transcription factor.

200

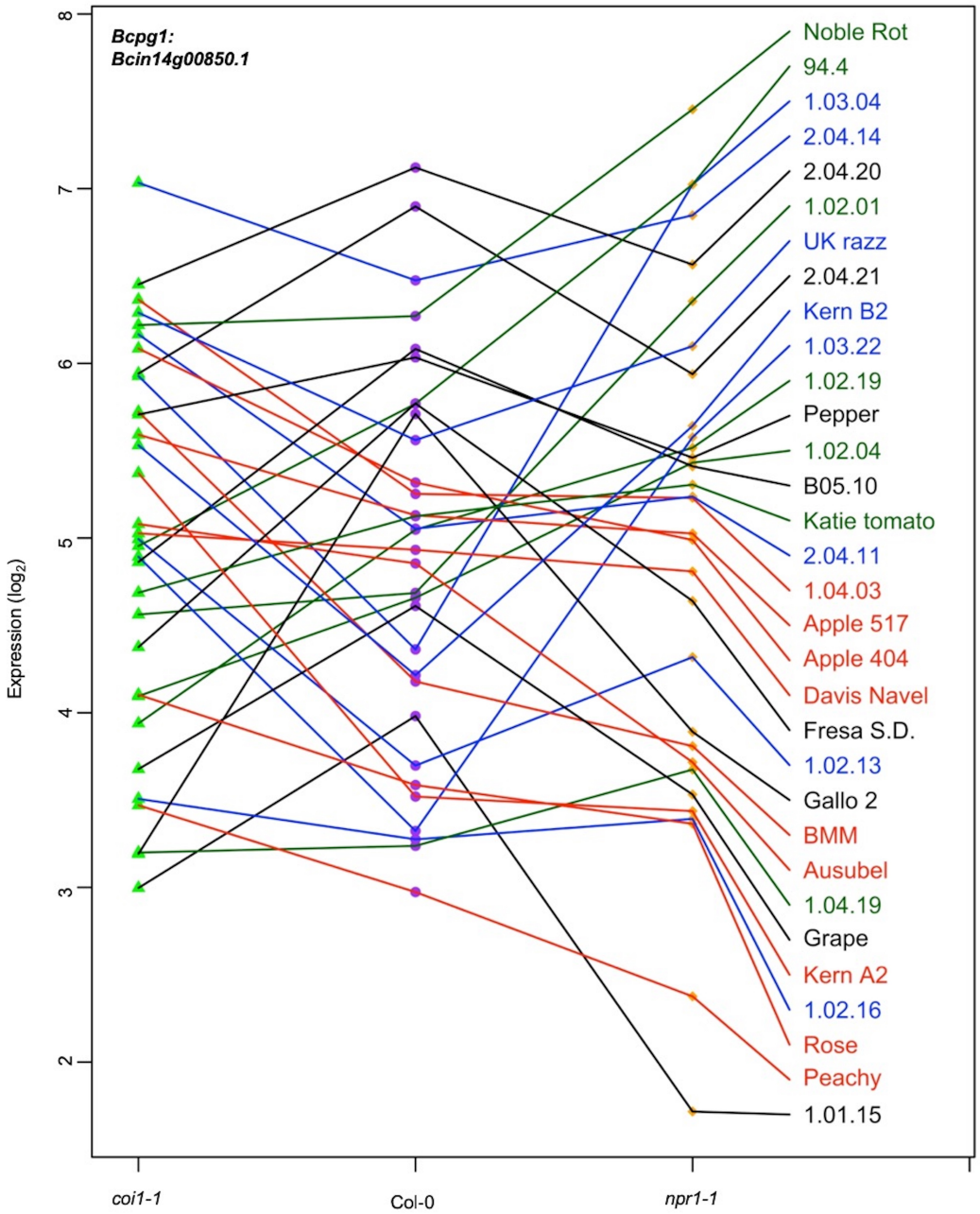

Figure 3. Expression profiles of an endopolygalacturonase gene *Bcpg1* from diverse *B. cinerea* isolates across Arabidopsis genotypes. Rank plot shows the relationship of *Bcpg1* expression from 32 diverse *B. cinerea* isolates (right) across three Arabidopsis genotypes (x axis). Three Arabidopsis genotypes are wild-type Col-0 (purple dot), jasmonate insensitive mutant *coi1-1* (green triangle), and salicylic acid mutant *npr1-1* (orange diamond). The model-corrected means ($\log_2$) for the transcript of *Bcpg1* (*Bcin14g00850.1*) encoding an endopolygalacturonase gene are utilized for plotting. The transcript expression levels from the same isolate across three Arabidopsis genotypes are connected with a colored line. The names of 32 isolates are represented with the same colored lines as induced *Bcpg1* expression levels. Black lines indicate the expression levels of *Bcpg1* are higher in *coi1-1* and *npr1-1* than in Col-0. Red lines indicate the higher expression levels of *Bcpg1* in *coi1-1* but lower in *npr1-1*. Blue lines indicate the highest expression levels of *Bcpg1* are in Col-0. Dark green lines indicate the higher expression levels of *Bcpg1* in *npr1-1* but lower in *coi1-1*.

201

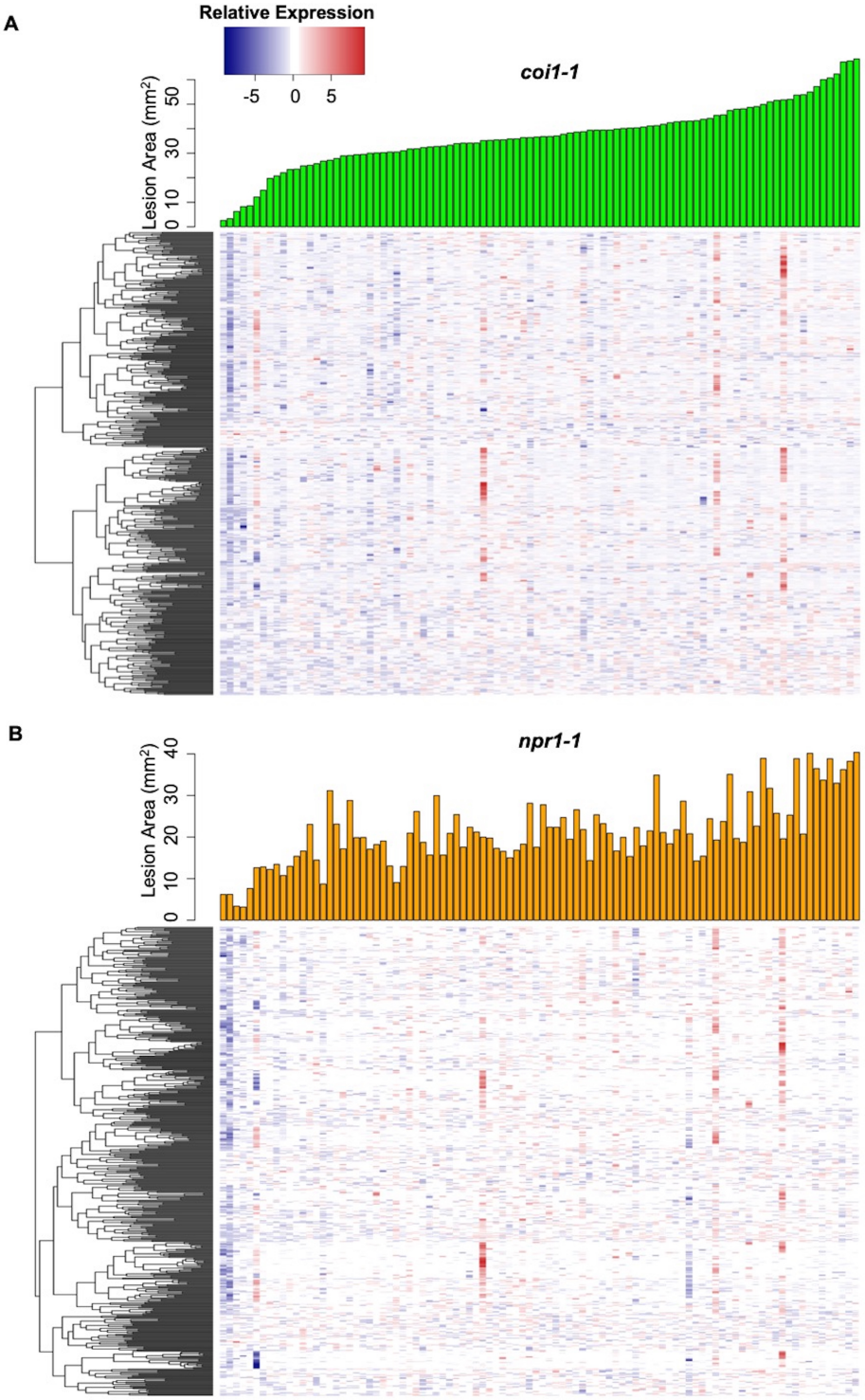

Figure 4. Interaction effects of host genotypes and pathogen isolates on *B. cinerea* transcriptome. Hierarchical clustering of relative expression of 500 genes from 96 *B. cinerea* isolates infection on Arabidopsis mutants *coi1-1* (A) or *npr1-1* (B) are plotted based on pairwise comparison of pathogen gene expression under Col-0. The 500 *B. cinerea* genes with highest broad-sense heritability (H^2) of host X pathogen were used for analysis. Lesion area induced by 96 isolates are compared under *coi1-1* (orange bar plot) and *npr1-1* (green bar plot).

202

203 pathogens transcriptional responses are influenced by a blend of the pathogens' natural variation
204 and its interaction with the host, while there is less evidence for the host's defense responses to
205 unilaterally affect *B. cinerea*. Future work will hopefully assess how this extends to other host-
206 pathogen systems.

207 **Identification of Virulence Factors Among the Early *B. cinerea* Transcripts**

208 This data set also allows us to test for specific *B. cinerea* transcripts whose early expression is
209 associated with later lesion development. These genes can serve as potential biomarkers of
210 overall pathogen virulence and may elucidate the functional mechanisms driving early virulence
211 in the interaction. To find individual pathogen transcripts link with lesion development, we
212 conducted a genome-wide false discovery rate-corrected Spearman's rank correlation analysis
213 between 72HPI lesion area and individual *B. cinerea* transcripts accumulation at 16HPI. We
214 identified 2,521 genes (22% of *B. cinerea* predicted gene models) with significant positive
215 correlations and 114 genes (1% of *B. cinerea* predicted gene models) with significant negative
216 correlations to lesion area across three Arabidopsis genotypes, respectively (P-value < 0.01,
217 Supplemental Data Set 6). The top 20 positively correlated *B. cinerea* genes contained all seven
218 genes involved in BOT biosynthesis (Deighton et al., 2001; Colmenares et al., 2002; Wang et
219 al., 2009; Rossi et al., 2011; Ascari et al., 2013; Porquier et al., 2016). In addition to
220 phytotoxins, more than 30 genes of the top 100 lesion-correlated genes encode plant cell wall
221 degrading enzymes, i.e., glucosyl hydrolases, carbohydrate esterases, cellobiose dehydrogenases
222 and *Bcpg1* (Figure 3 and Supplemental Data Set 6) (Gerbi et al., 1996; Zamocky et al., 2006;
223 Cantarel et al., 2009; Van Vu et al., 2012; Igarashi et al., 2014; Ingo Morgenstern et al., 2014;
224 Blanco-Ulate et al., 2014; Tien-chye Tan et al., 2015; Courtade et al., 2016; Nelson et al.,
225 2017; Pérez-Izquierdo et al., 2017). Additionally, 10 of the top 100 lesion-correlated genes were

226 annotated as putative peptidase activities, which are critical for fungal virulence (Movahedi et
227 al., 1991; Poussereau, Creton et al., 2001; Poussereau, Gente et al., 2001; ten Have et al.,
228 2004; ten Have et al., 2010). A final classical virulence gene in the top 100 gene list is *Bcoah*
229 (*Bcin12g01020*) encoding oxaloacetate acetyl hydrolase, which is a key enzyme in oxalic acid
230 biosynthesis that positively contributes to virulence (Figure 3-figure supplemental 1 and
231 Supplemental Data Set 6) (Greenberg et al., 1994; Williamson et al., 2007; Walz et al., 2008;
232 Schumacher et al., 2012; Schumacher et al., 2015; Tayal et al., 2017). In addition, this method
233 identified 37 of the top 100 lesion-correlated genes with no gene ontology (GO) terms, which
234 likely represent unknown virulence mechanisms (Supplemental Data Set 6). Thus, this approach
235 readily creates new hypothesis about known and novel pathogen virulence functions.

236 ***In Planta* Virulence Gene Co-expression Networks (GCNs) in *B. cinerea***

237 To develop a systemic view of fungal pathogen *in planta* gene expression, we used a co-
238 expression approach to identify *B. cinerea* networks that associated with growth and virulence *in*
239 *planta*. Using solely *B. cinerea* transcriptome at 16HPI from Arabidopsis Col-0 WT infected
240 leaves, we calculated Spearman's rank correlations of gene counts across all *B. cinerea* isolates,
241 filtered gene pairs with correlation greater than 0.8. We then used the filtered gene pairs as input
242 to construct GCNs. We identified ten distinct GCNs containing more than five *B. cinerea* genes
243 (Figure 5, Supplemental Table 1, Figure 5-figure supplemental 1 and Supplemental Data Set 7).
244 The largest GCN with 242 genes contains members responsible for phospholipid synthesis,
245 eiosome function, and membrane-associated stress signaling pathways (Figure 5-
246 Vesicle/virulence). The biological function of this GCN suggests its role in fungal membrane-
247 and vesicle-localized processes, which are normally involved with general hyphae growth,
248 fungal cell wall deposition, and exudation of fungal toxins to the intercellular space

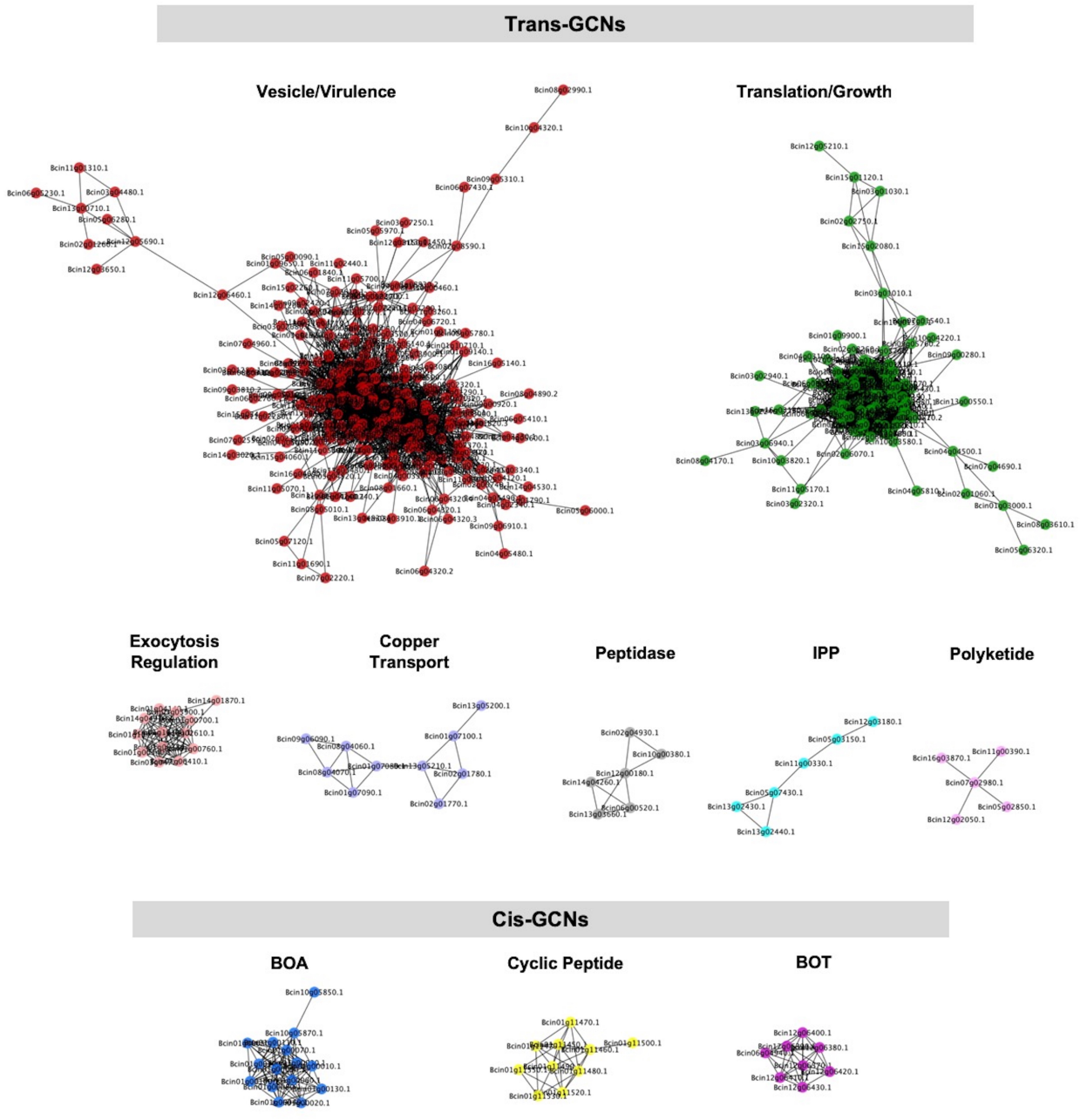

Figure 5. Gene co-expression networks identified from *B. cinerea* transcriptomic responses to Arabidopsis wild-type Col-0 immunity. Ten gene co-expression networks (GCNs) with more than five nodes were identified from 96 *B. cinerea* isolates infecting on Arabidopsis wild-type Col-0. The similarity matrix is computed using Spearman's rank correlation coefficient. Nodes with different colors represent *B. cinerea* genes condensed in GCNs with different biological functions. Edges represent the Spearman's rank correlation coefficients between gene pairs. Trans- and cis-GCNs means GCNs are regulated by trans- and cis-regulatory elements, respectively. GCNs were named after their biological functions, which were determined by hub and bottleneck genes within each network. GCNs are: vesicle/virulence (red), translation/growth (green), exocytosis regulation (pink), cyclic peptide (yellow), peptidase (gray), isopentenyl pyrophosphate (IPP, turquoise), polyketide (violet), botcinic acid (BOA, blue), copper transport (slate blue), botrydial (BOT, purple).

249

250 (Supplemental Data Set 7). The second largest network contains 128 genes that were entirely
251 associated with translation and protein synthesis (Figure 5-Translation/growth and Supplemental
252 Data Set 7). Of the smaller GCNs identified (5-20 genes), five networks were identified with
253 genes distributed across *B. cinerea* 16 chromosomes, suggesting that these GCNs arise from
254 coordinated trans-regulation (Figure 5-Trans-networks and Figure 5-figure supplemental 1D, 1F,
255 1H-1G). These networks are associated with diverse array of virulence functions, including the
256 regulation of exocytosis, copper transport, the production of peptidases and isoprenoid
257 precursors (IPP), and polyketide secretion.

258 In contrast to the whole-genome distributed GCNs, three of the smaller GCNs were
259 predominantly comprised of genes tandemly clustered within a single chromosome with no or a
260 few genes on other chromosomes (Figure 5-BOA, -Cyclic Peptide, -BOT, Figure 5-figure
261 supplemental 1C, 1E, and 1G). A functional analysis showed that all of the genes within these
262 networks encoded known or putative biosynthetic enzymes for specialized metabolic pathways.
263 For example, seven genes responsible for BOT biosynthesis cluster on chromosome 12 and form
264 a small GCN with a Zn(II)2Cys6 transcription factor that is specific to the pathway (Figure 6A,
265 6B, Figure 5-figure supplemental 1G and Supplemental Data Set 7) (Siewers et al., 2005;
266 Pinedo et al., 2008; Urlacher and Girhard, 2012; Moraga et al., 2016). Similarly, all 13 genes
267 involved in BOA biosynthesis cluster in Chromosome 1 and form a highly connected GCN
268 (Figure 5-BOA, Figure 6E, Figure 5-figure supplemental 1C and Supplemental Data Set 7)
269 (Dalmais et al., 2011; Porquier, Antoine et al., 2019). In addition to previously characterized
270 secondary metabolic pathways, we identified an uncharacterized set of ten genes that cluster on
271 Chromosome 1 (Figure 5-Cyclic Peptide, Figure 6F, Figure 5-figure supplemental 1E and
272 Supplemental Data Set 7). These genes share considerable homology with enzymes related to

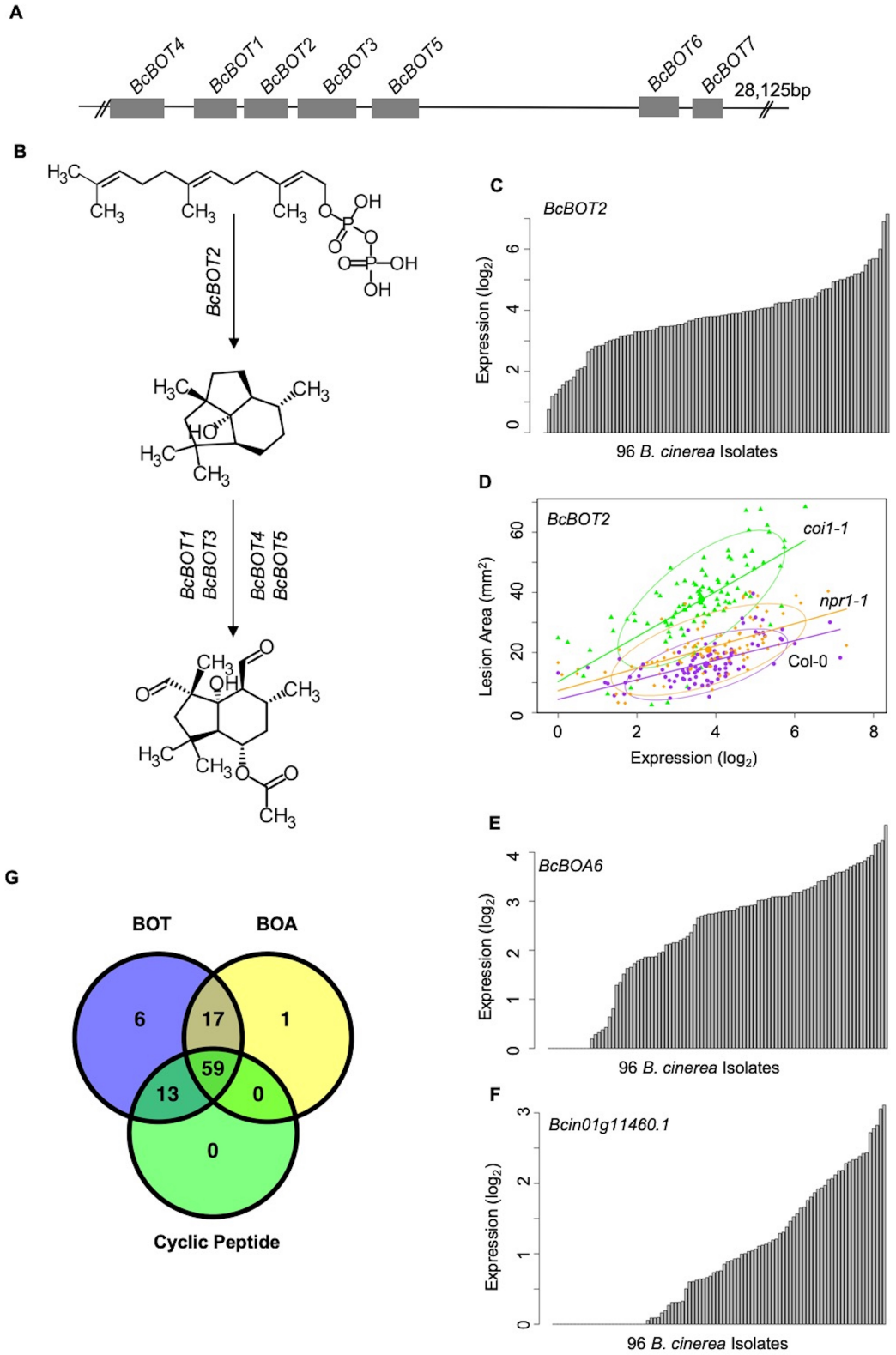
A
BcBOT4
BcBOT1
BcBOT2
BcBOT3
BcBOT5
BcBOT6
BcBOT7
28,125bp
B
BcBOT2
BcBOT1
BcBOT3
BcBOT4
BcBOT5
C
BcBOT2
Expression (log2)
96 B. cinerea Isolates
D
BcBOT2
coi1-1
npr1-1
Col-0
Lesion Area (mm2)
Expression (log2)
E
BcBOA6
Expression (log2)
96 B. cinerea Isolates
F
Bcin01g11460.1
Expression (log2)
96 B. cinerea Isolates
G
BOT
BOA
6
17
1
59
13
0
0
Cyclic Peptide

273

Figure 6. Variation of transcripts accumulation for secondary metabolites production across diverse *B. cinerea* isolates. Expression profiles of genes responsible for botrydial, botcinic acid, cyclic peptide production across 96 isolates under Arabidopsis wild-type Col-0 are shown. **(**A) Schematic shows the genomic locus of seven botrydial (BOT) biosynthesis genes clustered together. Exons are represented by gray boxes. Introns and intergenic regions are represented by the grey line. Seven BOT genes are: *BcBOT1, BcBOT3* and *BcBOT4,* encoding a cytochrome P450 monooxygenase, respectively; *BcBOT2* encoding a sesquiterpene cyclase; *BcBOT5* encoding an acetyl transferase; *BcBOT6* encoding a Zn(II)2Cys6 transcription factor, *BcBOT7* encoding a dehydrogenase reductase. (B) BOT biosynthesis pathway in *B. cinerea*. (C) Bar plots compare expression variation of *BcBOT*2 across 96 *B. cinerea* isolates in responding to Arabidopsis wild-type Col-0 immunity. The model-corrected means (log_2) of transcripts were used for plotting. (D) Scatter plot illustrates the positive correlations between lesion area and accumulation of *BcBOT2* transcript across the 96 isolates in response to varied Arabidopsis immunities. Model-corrected lesion area means were estimated for three Arabidopsis genotypes at 72-hours post-infection with 96 *B. cinerea* isolates. The three Arabidopsis genotypes are labeled next to the confidence ellipse curves: wild-type Col-0 (purple dot), jasmonate insensitive mutant *coi1-1* (green triangle), and salicylic acid mutant *npr1-1* (orange diamond). The 90% confidence ellipse intervals are plotted for each Arabidopsis genotype for reference. Linear regression lines: Col-0: y = 3.2532x + 4.4323, *P* = 1.008e-10, Adjusted R^2 = 3.3537; *coi1-1*: y = 7.4802x + 10.3289, *P* = 7.895e-15, adjusted R^2 = 0.4700; *npr1-1*: y = 3.7086x + 7.3487, *P* = 2.425e-11, adjusted R^2 = 0.3726. (E) and (F) Bar plots compare expression variation of *BcBOA6* in botcinic acid (BOA) pathway and *Bcin01g11460.* in cyclic peptide pathway across 96 *B. cinerea* isolates in response to Arabidopsis wild-type Col-0 immunity. (G) Venn diagram illustrates the number of *B. cinerea* isolates with the ability to induce BOT, BOA, and cyclic peptide.

cyclic peptide biosynthesis and may represent a novel secondary metabolic pathway in *B. cinerea* (Supplemental Data Set 7). The expression of these pathways *in planta* was extremely variable among the isolates and included some apparent natural knockouts in the expression of the entire biosynthetic pathway (Figure 6G and Supplemental Data Set 1). Isolate 94.4 was the sole genotype lacking the entire BOT pathway, while 19 isolates and 24 isolates did not transcribe respectively the BOA and the putative cyclic peptide pathways (Figure 6E to 6G and Supplemental Data Set 1). We decomposed the expression of these pathways into expression vectors, referred to as eigengenes, using a principle component analysis and used a linear mixed model to test for a relationship between early expression of secondary metabolic pathways and later lesion area. This showed a significant relationship between the expression of BOT and BOA pathways and lesion area measured at 72HPI (Supplemental Table 2). In contrast, the putative cyclic peptide pathway was only associated with lesion development in a BOT-dependent manner, suggesting that it may have a synergism to BOT (Supplemental Table 2). Thus, *in planta* analysis of the fungal transcriptome can identify known and novel potential virulence mechanisms and associate them with the resulting virulence.

290 **Covariation of Fungal Virulence Networks Under Differing Plant Immune Responses**

291 The *B. cinerea* GCNs measured within Arabidopsis WT provide a reference to investigate how
292 phytohormone-signaling in host innate immunity may shape the pathogen's transcriptional
293 responses during infection. Comparing the *B. cinerea* GCN membership and structure across the
294 three Arabidopsis genotypes (WT, *coi1-1*, and *npr1-1*) showed that the core membership within
295 networks was largely maintained but the specific linkages within and between GCNs were often
296 variable (Figure 7, Supplemental Table 1, Figure 7-figure supplemental 1, 2, 3, and
297 Supplemental Data Set 7). For example, the two largest *B. cinerea* GCNs in WT developed
298 multiple co-expression connections during infection in the JA-compromised *coi1-1* host (Figure
299 7 and Supplemental Table 1). In contrast, some GCNs have a highly robust structure across three
300 host genotypes, including three GCNs associated with BOT, BOA and cyclic peptide production,
301 and GCNs associated with exocytosis regulation, copper transport, and peptidase activity
302 (Supplemental Table 1, Figure 7-figure supplemental 1, 2, 3, and Supplemental Data Set 7). In
303 addition, we also identified additional small GCNs that demonstrated host specificity in *coi1-1*
304 (Supplemental Figure 4 and Supplemental Data Set 7). In particular, there were four small GCNs
305 that are associated with plant cell wall degradation, siderophores, glycolysis, ROS, and S-
306 adenosylmethionine biosynthesis (Figure 7-figure supplemental 3). Thus, the coordinated
307 transcriptional responses of *B. cinerea* GCNs are at least partially dependent on variation in the
308 host immune response.

309 Host immunities showed different impacts on expression profiles of genes condensed in
310 individual *B. cinerea* GCNs (Figure 7-figure supplemental 4). Compared with WT, expression
311 profiles of genes within the largest membrane/vesicle virulence GCN were elevated in the SA-

312 and JA-compromised Arabidopsis mutants on average (Figure 7-figure supplemental 4A).
313 Fungal genes associated with copper transport and polyketide production were upregulated under
314 SA-compromised host immunity (Figure 7-figure supplemental 4F and 4J). Whereas, members
315 of GCNs responsible for plant cell wall degradation and siderophore biosynthesis were
316 upregulated under JA-compromised host immunity (Figure 7-figure supplemental 4K and 4L).
317 Finally, GCNs associated with BOT and exocytosis regulation showed robust gene expression
318 profiles across all three Arabidopsis genotypes (Figure 7-figure supplemental 4D and 4G). The
319 above observation indicates host immunity influences the *B. cinerea* transcriptional response of
320 *B. cinerea* and suggests that *B. cinerea* isolates have varied abilities to tailor virulence strategy in

321 response to host immunity.

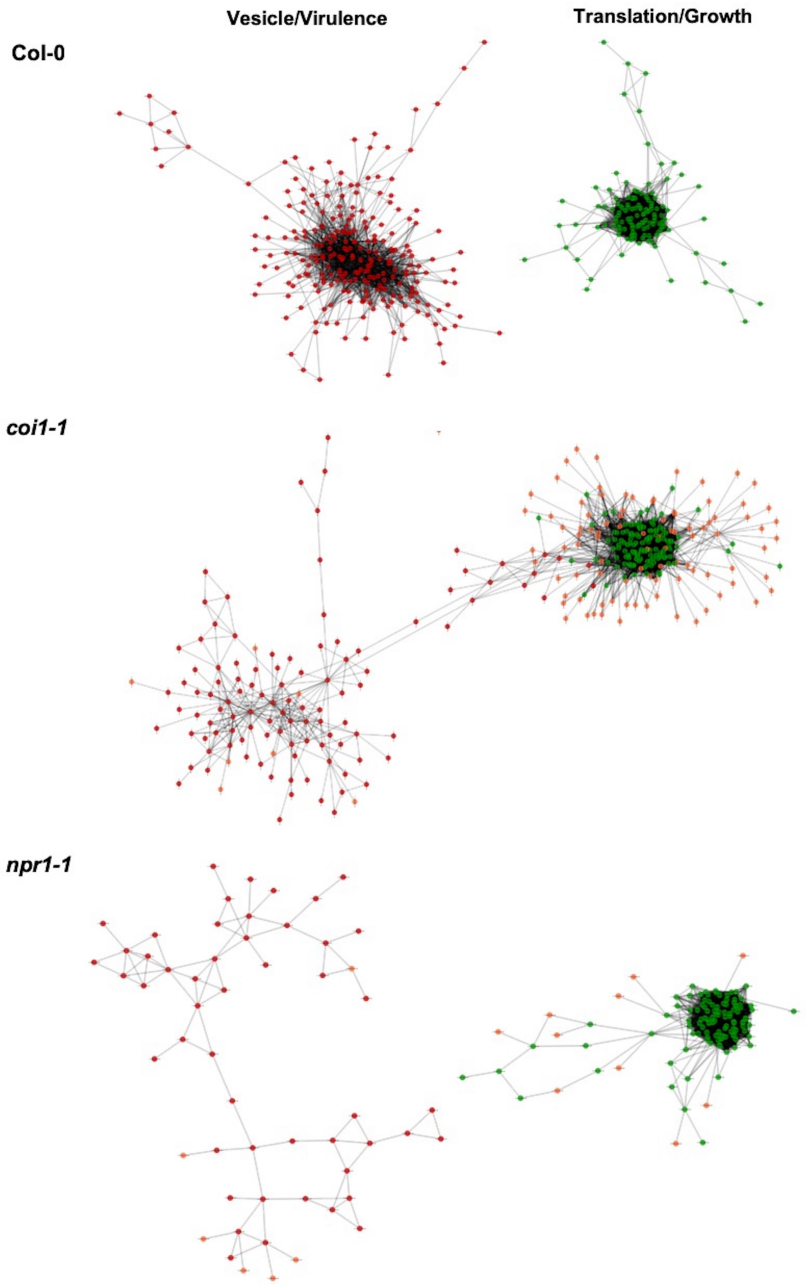

Figure 7. Comparison of plasticity of *B. cinerea* gene co-expression network under vaired host immunity. *B. cinerea* gene co-expression networks (GCNs) of vesicle/virulence (red) and translation/growth (green) identified under three Arabidopsis genotypes are compared. Three Arabidopsis genotypes are wild-type Col-0, jasmonate insensitive mutant *coi1-1*, and salicylic acid mutant *npr1-1*. Nodes marked with red and green colors represent *B. cinerea* genes condensed in GCNs with different biological functions. The same node condensed in GCNs across three Arabidopsis genotypes was marked with same color. Nodes specificaly condensed in GCNs under two mutants *coi1-1* and *npr1-1* background are marked with orange color. Edges represent the Spearman's rank correlation coefficients between gene pairs.

322

323 **Cross-kingdom Co-transcriptomic Networks Revealed Direct Gene-for-gene Interaction**

324 To test the interaction between individual genes from two organisms, we generated Arabidopsis-
325 *B. cinerea* GCNs using co-transcriptome data under each host genotype. We calculated
326 Spearman's rank correlation coefficients among 23,898 Arabidopsis transcripts and 9,284 *B.*
327 *cinerea* transcripts. This approach identified three cross-kingdom GCNs (CKGCNs) under
328 Arabidopsis WT and JA- or SA-compromised two mutants (Figure 8, Supplemental Table 5, and
329 Supplemental Data Set 8). Under Arabidopsis WT, a total of 54 hub genes were identified, half
330 from *B. cinerea* and half from Arabidopsis. Furthermore, CKGCNs contain a majority of genes
331 in the BOT GCN and a small proportion of genes in the vesicle/virulence GCN (Figure 8-figure
332 supplemental 1C, 1G, 1F and 1H). For plants, CKGCNs contain a majority of genes from
333 Arabidopsis Defense/camalexin GCN (Figure 8-figure supplemental 1B). These CKGCNs also
334 contain genes associated with extensive host defense responses, i.e., genes encoding membrane-
335 localized leucine-rich repeat receptor kinases (LRR-RKs), stress signal sensing and transduction,
336 tryptophan-derived phytoalexin production, regulation of cell death, cell wall integrity, nutrition
337 transporters, etc. (Supplemental Data Set 8). The topological structure and gene content of the
338 CKGCNs shifted across the three Arabidopsis genotypes (Figure 8). These changes illustrate
339 how the host genotype can influence the intercommunication in the host-pathogen interaction.

A Col-0

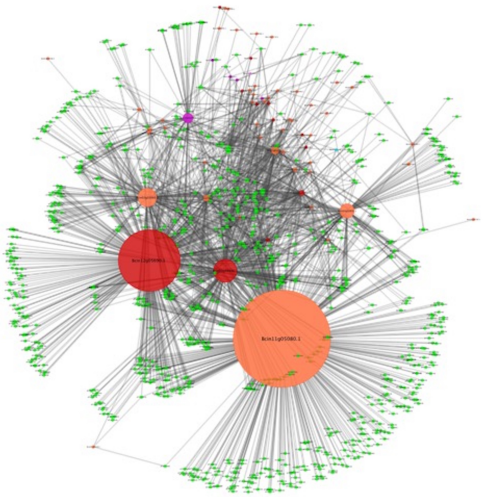

B *coi1-1*

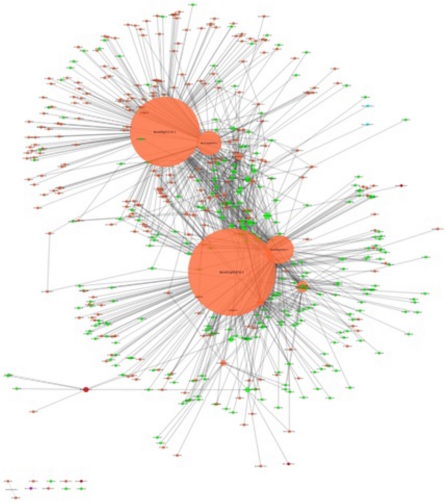

C *npr1-1*

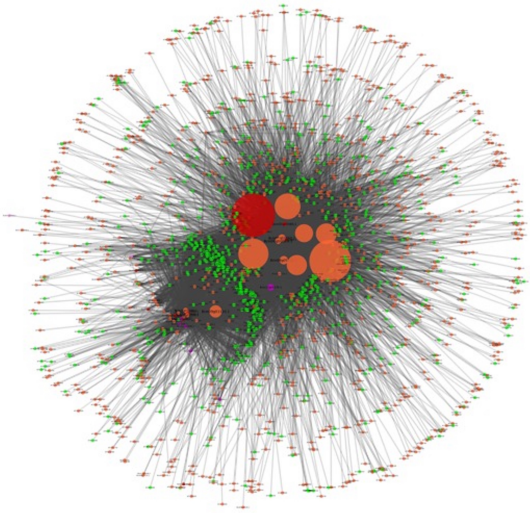

340

Figure 8. Cross-kingdom Arabidopsis-*B. cinerea* gene co-expression networks. Three Arabidopsis genotypes are wild-type Col-0, jasmonate insensitive mutant *coi1-1*, and salicylic acid insensitive mutant *npr1-1*. Green nodes represent Arabidopsis genes. Orange, red and violet nodes represent *B. cinerea* genes. Nodes with red and violet colors are condensed in *B. cinerea* vesicle/virulence and BOT gene co-expression networks, respectively. The degree of a node is shown by the size of a node. Edges represent the Spearman's rank correlation coefficients between gene pairs.

A Dual Interaction Network Reveals Fungal Virulence Components Targeting Host Immunity

To begin assessing how two species influence each other's gene expression during infection, we constructed a co-transcriptome network using both the host- and pathogen-derived GCNs (Figure 9 and Figure 9-figure supplemental 1). We converted the ten *B. cinerea* GCNs and the four Arabidopsis GCNs into eigengene vectors that capture the variation of the general expression of all genes within a GCN into a single value (Zhang et al., 2017). The Arabidopsis GCNs were defined in response to this same transcriptome but by using solely the host transcripts. Of these four Arabidopsis GCNs, one is largely comprised of genes in Defense/Camalexin signaling, two are linked to different aspects of photosynthesis and the fourth is largely comprised of host genes in cell division. We calculated Spearman's rank coefficients among each GCN eigengene pairs without regard for the species. In this dual transcriptome network, the Arabidopsis/*B. cinerea* GCN eigengenes are displayed as nodes and positive/negative correlations between the GCNs as edges (Figure 9 and Figure 9-figure supplemental 1). Of the host-derived GCNs, the Arabidopsis Defense/camalexin and Photosystem I (PSI) GCNs have a higher degree of centrality within the dual interaction network, suggesting that they have the most interactions with *B. cinerea* GCNs. The fungal GCNs highest degrees were associated with the exocytosis regulation, BOT, and IPP, which further illustrating the importance of specialized metabolism exudation in pathogen virulence. Interestingly, fungal GCNs (copper transport, exocytosis regulation, BOT and IPP biosynthesis) that were positively correlated with the host Defense/camalexin GCN showed

362 negative correlations with PSI eigengene. The opposite relationships between pathogen- and
363 host-GCNs suggest that these fungal GCNs may target plant PSI while the plant counters this
364 attack using the Defense/camalexin GCN.

365 To test if these connections were dependent upon the host immunity, we used the eigengene
366 values derived from fungal GCNs to conduct mixed linear modelling of how they were linked to
367 variation in the host genotype and/or host GCNs (Supplemental Table 3 and 4). Some *B. cinerea*
368 GCNs (Vesicle/virulence and TSL/growth, etc.) were affected by variation in the host genotypes
369 but others showed host-independent manner (BOT, copper transport, etc.). Critically, the
370 connections between pathogen- and host-GCNs were largely independent of the host genotypes,
371 suggesting that the dual interaction network is a relatively robust structure (Supplemental Table
372 3 and 4). Collectively, pathogen virulence and host immunity GCNs showed complex
373 connections within dual interaction network identified from co-transcriptome data, suggesting
374 functional relationships between host defense and pathogen virulence mechanisms for future
375 experimentation.

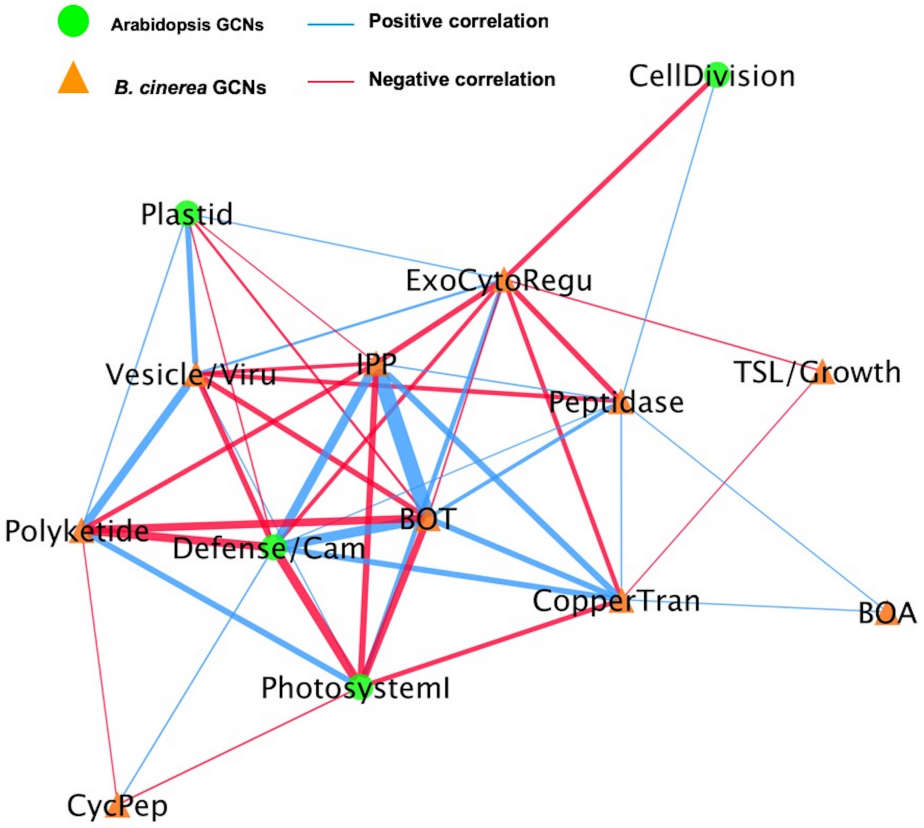

Figure 9. A dual interaction network reveals links between Arabidopsis immunity and *B. cinerea* virulence. A dual interaction network was constructed using gene co-expression networks (GCNs) from Arabidopsis and *B. cinerea* co-transcriptome. The first eigenvectors were derived from individual GCNs and used as input to calculate Spearman's rank correlation coefficiency between GCN pairs. Green dots and orange triangles represent Arabidopsis immune- and *B. cinerea* virulence-GCNs, respectively. Blue and red lines (edges) represent the positive and negative Spearman's rank correlation coefficients between GCN pairs, respectively. The thickness of line signifies the correlational strength.

Germinations Influence on the Co-Transcriptome

One potential complicating factor that may influence the co-transcriptome is variation in germination of the spores between *B. cinerea* strains. The lack of universal genomic patterns for host x pathogen interactions in the co-transcriptome argues that germination is not causing global effects on the co-transcriptome (Figures 3 and 4). To begin examining how variation in *B. cinerea* spore germination may influence the co-transcriptome and our identified link to

383 virulence, we investigated the germination of 19 isolates. This showed that there was some
384 variation in germination with all but a few isolates germinating within the 6-7 hours' time frame
385 at room temperature (Figure 9-figure supplemental 2). To extend this to an *in planta* analysis, we
386 utilized an existing microarray study on *B. cinerea* germination to develop an eigengene that
387 estimates the relative germination between the strains using the *in planta* transcriptomic data
388 (Leroch et al., 2013). We then used this *in planta* estimation of germination to test if our
389 previously identified co-transcriptome to virulence links were altered by controlling for
390 germination. Using linear models, we ran the same test whereby the major *B. cinerea* GCNs
391 were tested for a link to virulence although this time, we included the germination eigengene as a
392 co-variate. This analysis showed that the *in planta* estimation of germination significantly
393 associated with virulence. Critically, even with germination taken into account, all the *B. cinerea*
394 networks remained significantly associated to lesion area. Some GCNs link, i.e. BOT and BOA,
395 were largely unaffected by the germination estimates (Supplemental Table 6), showing that some
396 aspects of virulence are independent of spore germination. In contrast other GCNs like the
397 vesicle linked GCN had their link to virulence decreased but not abolished by including the
398 germination co-variate. Thus, while spore germination plays a role in our measurement of the
399 plant-pathogen interaction, it is only one of multiple factors influencing the co-transcriptome and
400 is not imparting a dominant global influence on the observed patterns.

401 **DISCUSSION**

402 In recent decades, improvements in the understanding of the molecular basis of plant-pathogen
403 dynamics have facilitated breeding strategies for disease resistance in a variety of crop species.
404 However, breeding for disease resistance remains difficult for crops susceptible to pathogens that

405 harbor diverse polygenic virulence strategies targeting multiple layers and components of the
406 plant innate immune system (Corwin and Kliebenstein, 2017). In this study, we investigated the
407 transcriptome profiles at an early infection stage both within *B. cinerea* and across the interaction
408 within the Arabidopsis-*B. cinerea* pathosystem. This showed that the transcriptional virulence
409 strategy employed by *B. cinerea* is dependent both on fungal genotype and the functional
410 response of the host plant's immune system. We identified a batch of early *B. cinerea* transcripts
411 associated with later lesion development and several pathogen GCNs responsible for mediating
412 virulence in *B. cinerea*, including a potential specialized metabolic pathway of cyclic peptide
413 virulence factor. Lastly, we constructed a co-transcriptome network that revealed known and
414 novel fungal virulence components coordinated expressed with plant host GCNs during
415 infection.

416 There are some potential limitations on the utility of cross-species GCNs. Predominantly, they
417 are a correlational approach where links are made between host and pathogen transcriptional
418 changes. While this leads to the development of new hypothesis, it will equally require future
419 validation efforts to assess if these are direct or indirect relationships. Additionally, the cross-
420 species GCN approach as implemented in this work does not distinguish between host/pathogen
421 cells that are directly interacting versus those that are having long-distance responses. An
422 important future avenue will be to integrate cell-specific RNA sequencing approaches to better
423 delineate what are the responses within host/pathogen cells that are directly interacting versus the
424 long-distance responses. This would greatly increase the power of elucidating direct versus
425 indirect effects in this system.

426 **Secondary Metabolites May Mediate Plant and Fungus Transcriptomic Interactions**
427 **During Infection**

428 Necrotrophic pathogen *B. cinerea* has evolved an arsenal of virulence strategies to establish
429 colonization and enhance infection within the plant host, including production of secondary
430 metabolites. The co-transcriptome approach shows that the expression of fungal specialized
431 pathways early in infection correlates with later lesion development (Supplemental Table 3).
432 Three secondary metabolite GCNs are clustered within the fungal genome and two of them
433 identified with pathway-specific transcription factors (Figure 6, Figure 7-figure supplemental 2,
434 3, and Supplemental Data Set 7). Further, the expression of these pathways displayed a large
435 range of phenotypic variation across the isolates (Figure 6G and Supplemental Data Set 1).
436 However, the topology and memberships of GCNs for the three pathways are largely insensitive
437 to variation in host immunity. Robustness to host immunity suggests that these GCNs are
438 somehow insulated from the host's immune response, possibly to protect toxin production from a
439 host counter-attack. The co-transcriptome approach showed the ability to identify known and
440 novel secondary metabolic pathways that mediate plant host and fungal pathogen interaction.

441 Importantly, the dual interaction networks provide hypothesis for pathogen-GCNs responsible
442 for fungal secondary metabolites production link to specific plant host-GCNs (Figure 9 and
443 Figure 9-figure supplemental 1). Specifically, the co-transcriptome approach revealed that *B.*
444 *cinerea* GCNs responsible for secondary metabolite production are positively associated with
445 plant immune responses and negatively associated with primary plant metabolism (Figure 9,
446 Supplemental Table 3 and 4). For example, the BOT GCN shows a strong positive correlation
447 with the Arabidopsis defense/camalexin GCN, suggesting that BOT production may directly

448 induce the host's defense system. Concurrently, the BOT GCN is negatively linked to the plant's
449 PSI GCN, suggesting that BOT may repress the plant's photosynthetic potential. Further work is
450 needed to test the direction of causality within the dual interaction network as it is possible that
451 the host's defense/camalexin network is responding to the PSI alteration, or vice versa.
452 Collectively, these results strongly implicate the ability of secondary metabolites biosynthesis to
453 mediate the interactions between pathogen virulence and plant host immunity at the
454 transcriptomic level. The co-transcriptome approach showed the potential to enable us to form
455 new hypotheses about how this linkage may occur.

456 **Fungal Virulence Components Correlated with Plant Immune Response**

457 In addition to secondary metabolite biosynthesis, the co-transcriptome identified a number of key
458 virulence mechanisms that could be mapped to the two species interaction. One key GCN is
459 enriched for genes involved in exocytosis associated regulation (Figure 5-Exocytosis regulation
460 and Supplemental Data Set 7). The exocytosis complex is responsible for delivery of secondary
461 metabolites and proteins to the extra-cellular space and plasma membrane in fungi (Colombo et
462 al., 2014; Rodrigues et al., 2015). Additionally, we found many *B. cinerea* genes associated
463 with secretory vesicles within the membrane/vesicle virulence GCN that likely serve a similar
464 function during infection (Figure 5-Vesicle/virulence and Supplemental Data Set 7). These
465 GCNs also provide support for the role of exocytosis-based spatial segregation of different
466 materials during fungal hyphae growth *in planta* (Samuel et al., 2015). The dual interaction
467 network suggests that the exocytosis regulation and membrane/vesicle virulence GCNs are
468 differentially linked to the Arabidopsis defense/camalexin GCN, indicating varied connections
469 between fungal secretory pathways and plant immune responses (Figure 9 and Supplemental

470 Table 3 and 4). Another conserved GCN in the *B. cinerea* species is associated with copper
471 uptake and transport (Figure 5-Copper transport, Figure 7-figure supplemental 1, 2, 3, and
472 Supplemental Data Set 7). Although copper is essential for *B. cinerea* penetration and redox
473 status regulation within plant tissues, further work is required to decipher the precise molecular
474 mechanism involved in acquisition and detoxification of copper. Thus, the co-transcriptome
475 approach can identify both known and unknown mechanisms and links within the host-pathogen
476 interaction.

477 **Fungal Virulence Transcriptomic Responses Are Partly Shaped by Host Immunity**

478 It is largely unknown how plant host immunity contributes to the transcriptomic behavior of the
479 fungus during infection. Even less is known about the role of genetic variation in the pathogen in
480 responding to, or coping with, the inputs coming from the host immune system. In the current
481 study, we found that the host immune system's effect on pathogen transcripts and GCNs was
482 largely via an interaction with the pathogens genotype (Figure 2, Figure 7, Figure 7-figure
483 supplemental 4, and Supplemental Data 5). For example, fungal GCNs associated with
484 membrane/vesicle virulence and fungal growth shifted drastically between the WT and *coi1-1* or
485 *npr1-1* Arabidopsis genotypes (Figure 7). In addition, some GCNs only appeared in specific
486 backgrounds. For example, those linked to siderophores and a polyketide production were only
487 identified during infection of the JA-compromised Arabidopsis mutant (Figure 7-figure
488 supplemental 4J and 4L). However, other fungal GCNs, like those involved in secondary
489 metabolism, were largely insensitive to variation in the host immunity (Figure 7-figure
490 supplemental 1, 2, 3, Supplemental Table 1, and Supplemental Data Set 7). Critically, the gene
491 membership of these GCNs is largely stable across the collection of pathogen isolates, even

492 while their expression level across the *B. cinerea* isolates is highly polymorphic (Supplemental
493 Data Set 7 and Figure 7-figure supplemental 4). This suggests that natural variation in the host
494 immunity and pathogen shapes how the co-transcriptome responds to host's immune system.
495 Further, the natural variation in the pathogen may be focused around these functional GCNs.

496 **Plant Disease Development Can Be Predicted by Early Transcriptome Data**

497 Plant disease development is an abstract phenomenon that is the result of a wide set of spatio-
498 temporal biological processes encoded by two interplaying species under a specific environment.
499 In current study, we used late stage lesion area as a quantitative indicator of *B. cinerea* virulence.
500 We have previously shown that early Arabidopsis transcriptomic response could be linked to
501 later lesion development (Zhang et al., 2017). Here, our findings suggest that the late-stage
502 disease development of a *B. cinerea* infection is determined during the first few hours of
503 infection by the interaction of plant immune and fungal virulence responses. It was possible to
504 create a link between early transcripts' accumulation and late disease development using solely
505 the *B. cinerea* transcriptome (Figure 1 and Supplemental Data Set 6). This could be done using
506 either individual pathogen genes, GCNs, or more simply the total fraction of transcripts from the
507 pathogen. As the transcriptomic data were from plant leaf tissue only 16HPI, there is not a
508 significant amount of pathogen biomass and this is more likely an indicator of transcriptional
509 activity in the pathogen during infection. It is possible to develop these methods as possible
510 biomarkers for likely fungal pathogen caused disease progression.

511 **CONCLUSION**

512 By analyzing an early stage co-transcriptome of a *B. cinerea* population infection on
513 Arabidopsis, we identified a number of *B. cinerea* GCNs that contained a variety of virulence-
514 associated gene modules with different biological functions. The characterization of these GCNs
515 simultaneously identified mechanisms known to enhance *B. cinerea* virulence and implicated
516 several novel mechanisms not previously described in the Arabidopsis-*B. cinerea* pathosystem.
517 In addition, the plant-fungus co-transcriptome network revealed the potential interaction between
518 fungal pathogen- and plant host-GCNs. Construction of GCNs and dual networks shed lights on
519 the biological mechanisms driving quantitative pathogen virulence in *B. cinerea* and their
520 potential targets in the plant innate immune system.

521 **METHODS**

522 **Collection and Maintenance *B. cinerea* Isolates**

523 A collection of 96 *B. cinerea* isolates were selected in this study based on their phenotypic and
524 genotypic diversity (Denby et al., 2004; Rowe and Kliebenstein, 2007; Corwin et al., 2016;
525 Zhang et al., 2016; Zhang et al., 2017). This *B. cinerea* collection was sampled from a large
526 variety of different host origins and contained a set of international isolates obtained from labs
527 across the world, including the well-studied B05.10 isolate. A majority of isolates are natural
528 isolates that isolated from California and can infect a wide range of crops. Isolates are
529 maintained in -80°C freezer stocks as spores in 20% glycerol and were grown on fresh potato
530 dextrose agar (PDA) 10 days prior to infection.

531 **Plant Materials and Growth Conditions**

532 The Arabidopsis accession Columbia-0 (Col-0) was the wildtype background of all Arabidopsis
533 mutants used in this study. The three Arabidopsis genotypes used in this study included the WT
534 and two well-characterized immunodeficient mutants, *coi1-1* and *npr1-1*, that abolish the major
535 JA- or SA-defense perception pathways, respectively (Cao et al., 1997; Xie et al., 1998; Xu, L.
536 et al., 2002; Pieterse and Van Loon, 2004). All plants were grown as described previously
537 (Zhang et al., 2017). Two independent randomized complete block-designed experiments were
538 conducted and a total of 90 plants per genotype were grown in 30 flats for each experiment.
539 Approximately 5 to 6 fully developed leaves were harvested from the five-week old plants and
540 placed on 1% phytoagar in large plastic flats prior to *B. cinerea* infection.

541 **Inoculation and Sampling**

542 We infected all 96 isolates onto each of the three Arabidopsis genotypes in a random design with
543 6-fold replication across the two independent experiments. A total of twelve infected leaves per
544 isolate/genotype pair were generated. For inoculation, all *B. cinerea* isolates were cultured and
545 inoculated on three Arabidopsi*s* genotypes as described previously (Denby et al., 2004; Corwin
546 et al., 2016; Zhang et al., 2017). Briefly, frozen glycerol stocks of isolate spores were first used
547 for inoculation on a few slices of canned peaches in petri plates. Spores were collected from one-
548 week-old sporulating peach slices. The spore solution was filterred and the spore pellet was re-
549 suspended in sterilized 0.5x organic grape juice (Santa Cruz Organics, Pescadero, CA). Spore
550 concentrations were determined using a hemacytometer and suspensions were diluted to
551 10spores/μL. Detached leaf assays were used for a high-throughput analysis of *B. cinerea*
552 infection, which has been shown to be consistent with whole plant assay (Govrin and Levine,
553 2000; Mengiste et al., 2003; Denby et al., 2004; Sharma et al., 2005; Windram et al., 2012).

554 Five-week old leaves were inoculated with 4μL of the spore solution. The infected leaf tissues
555 were incubated on 1% phytoagar flats with a humidity dome at room temperature. The
556 inoculation was conducted in a randomized complete block design across the six planting blocks.
557 All inoculations were conducted within one hour of dawn and the light period of the leaves was
558 maintained. Two blocks were harvest at 16HPI for RNA-Seq analysis. The remaining four
559 blocks were incubated at room temperature until 72HPI when they were digitally imaged for
560 lesion size and harvested for chemical analysis as described previously (Zhang et al., 2017).

561 **RNA-Seq Library Preparation, Sequencing, Mapping and Statistical Analysis**

562 Two *B. cinerea* infected leaf tissues of the six blocks were sampled at 16HPI for transcriptome
563 analysis, which resulted in a total of 1,052 mRNA libraries for Illumina HiSeq sequencing.
564 RNA-Seq libraries were prepared according to a previous method (Kumar et al., 2012) with
565 minor modifications (Zhang et al., 2017). Briefly, infected leaves were immediately frozen in
566 liquid nitrogen and stored at -80°C until processing. RNA extraction was conducted by re-
567 freezing samples in liquid nitrogen and homogenizing by rapid agitation in a bead beater
568 followed by direct mRNA isolation using the Dynabeads oligo-dT kit. First and second strand
569 cDNA was produced from the mRNA using an Invitrogen Superscript III kit. The resulting
570 cDNA was fragmented, end-repaired, A-tailed and barcoded as previously described. Adapter-
571 ligated fragments were enriched by PCR and size-selected for a mean of 300 base pair (bp) prior
572 to sequencing. Barcoded libraries were pooled in batches of 96 and submitted for a single-end,
573 50bp sequencing on a single lane per pool using the Illumina HiSeq 2500 platform at the UC
574 Davis Genome Center (DNA Technologies Core, Davis, CA).

575 **Transcriptomic Data Analysis**

576 Fastq files from individual HiSeq lanes were separated by adapter index into individual RNA-
577 Seq library samples. The quality of individual libraries was estimated for overall read quality and
578 over-represented sequences using FastQC software (Version 0.11.3,
579 www.bioinformatics.babraham.ac.uk/projects/). We conducted downstream bioinformatic
580 analysis, like reads mapping, normalization and nbGLM model analysis, using a custom script
581 from the *Octopus* R package (https://github.com/WeiZhang317/octopus). The mapping of
582 processed reads against Arabidopsis and *B. cinerea* reference genomes was conducted by Bowtie
583 1 (V.1.1.2, http://sourceforge.net/projects/bowtie-bio/files/bowtie/1.1.2/) using minimum
584 phred33 quality scores (Langmead et al., 2009). The first 10bp of reads was trimmed to remove
585 low quality bases using the fastx toolkit
586 (http://hannonlab.cshl.edu/fastx_toolkit/commandline.html). Total reads for each library were
587 firstly mapped against the Arabidopsis TAIR10.25 cDNA reference genome. The remaining un-
588 mapped reads were then aligned against *B. cinerea* B05.10 isolate cDNA reference genome
589 (Lamesch et al., 2010; Lamesch et al., 2012; Krishnakumar et al., 2015; Van Kan et al., 2017)
590 and the gene counts for both species were pulled from the resulting SAM files (Li et al., 2009).

591 For pathogen gene expression analysis, we first filtered genes with either more than 30 gene
592 counts in one isolate or 300 gene counts across 96 isolates. We normalized *B. cinerea* gene
593 counts data set using the trimmed mean of M-values method (TMM) from the *EdgeR* package
594 (V3.12) (Robinson and Smyth, 2008; Bullard et al., 2010; Robinson and Oshlack, 2010). We
595 then ran the following generalized linear model (GLM) with a negative binomial link function
596 from the MASS package for all transcripts using the following equation (Venables and Ripley,
597 2002):

598 $Y_{egai} = E_e + E_e(Gf_g) + E_e(Gf_g(Af_a)) + I_i + H_h + H_h * I_i$

599 where the main categorical effects E, I, and H are denoted as experiment, isolate genotype, and
600 plant host genotype, respectively. Nested effects of the growing flat (Gf) within the experimental
601 replicates and agar flat (Af) nested within growing flat are also accounted for within the model.
602 Model corrected means and standard errors for each transcript were determined for each
603 isolate/plant genotype pair using the lsmeans package (Russell V. Lenth, 2016). Raw *P*-values
604 for F- and Chi Square-test were determined using Type II sums of squares using *car* package
605 (Fox and Weisberg, 2011). *P*-values were corrected for multiple testing using a false discovery
606 rate correction (Benjamini Yoav and Yekutieli Daniel, 2001). Broad-sense heritability (H^2) of
607 individual transcripts was estimated as the proportion of variance attributed to *B. cinerea*
608 genotype, Arabidopsi*s* genotype, or their interaction effects.

609 **Gene Ontology Analysis**

610 GO analysis was conducted for several *B. cinerea* gene sets that were identified with high heritability,
611 correlated with lesion size, and condensed in network analysis. We first converted sequences of these *B.*
612 *cinerea* genes into fasta files using *Biostrings* and *seqRFLP* packages in R (Ding Qiong and Zhang
613 Jinlong, 2012; Pages et al., 2017). The functional annotation of genes was obtained by blasting the
614 sequences against the NCBI database using Blast2GO to obtain putative GO annotations (Conesa et al.,
615 2005; Gotz et al., 2008). The GO terms were compared to the official GO annotation from the *B.*
616 *cinerea* database (http://fungi.ensembl.org/Botrytis_cinerea/Info/Index) and those obtained by Blast2GO
617 analysis. The official gene annotations for host genes was retrieved from TAIR10.25
618 (https://apps.araport.org/thalemine/bag.do?subtab=upload).

619 ***B. cinerea* Gene Co-expression Network Construction**

620 To obtain a representative subset of *B. cinerea* genes co-expressed under *in planta* conditions,
621 we generated gene co-expression networks (GCNs) among genes in the *B. cinerea* transcriptome.
622 GCNs were generated using the model-corrected means of 9,284 *B. cinerea* transcripts from
623 individual isolate infection across three Arabidopsis genotypes. Only genes with average or
624 medium expression greater than zero across all samples were considered. This preselection
625 process kept 6,372 genes and those with negative expression values were adjusted to set
626 expression at zero before network construction. Spearman's rank correlation coefficients for each
627 gene pair was calculated using the *cor* function in R. Three gene-for-gene correlation similarity
628 matrixes were generated independently for each of the three Arabidopsis genotypes. Considering
629 the cutoff for gene-pair correlation usually generates biases of GCN structure and the candidate
630 gene hit, we utilized several cutoff threshold values at 0.75, 0.8, 0.85, and 0.9 to filter the gene
631 set. Comparing the structure and content of GCNs among those GCN sets using filtered gene set
632 as input, we selected the correlation threshold at 0.8. A total of 600, 700 and 494 *B. cinerea*
633 candidate genes passed the criterion under Arabidopsis WT, mutants *coi1-1* and *npr1-1*,
634 respectively. To obtain a representative subset of *B. cinerea* gene candidates across three host
635 genotypes, we selected gene candidates that presented across the above three gene subsets. This
636 process generated a gene set with 323 *B. cinerea* candidate genes that were common to each of
637 the plant genotype backgrounds and had at least 0.8 significant correlations. Using this gene set
638 as kernel, we extended gene candidate sets under each Arabidopsis genotype. The expanded *B.*
639 *cinerea* gene candidate set under individual Arabidopsis genotypes was further used as input for
640 gene co-expression network construction.

641 GCNs were visualized using Cytoscape V3.2.1 (Java version:1.8.0_60) (Shannon et al., 2003).
642 The nodes and edges within each network represent the *B. cinerea* genes and the Spearman's

643 rank correlations between each gene pair. The importance of a given node within each network
644 was determined by common network analysis indices, such as connectivity (degree) and
645 betweenness. Nodes with higher connectivity and betweenness were considered as hub and
646 bottleneck genes, respectively, and the biological functions of each network were determined by
647 the GO terms of hub and bottle neck genes using Blast2GO.

648 **Cross-kingdom Arabidopsis-*B. cinerea* Gene Co-expression Network Construction**

649 We used model-corrected means of transcripts from three Arabidopsis host genotypes and 96 *B.*
650 *cinerea* isolates to construct the cross-kingdom Arabidopsis-*B. cinerea* GCNs. Model-corrected
651 means of 23,959 Arabidopsis transcripts and 6,372 *B. cinerea* transcripts derived from two
652 negative binomial linked generalized linear models were served as input data sets (Zhang et al.,
653 2017). Spearman's rank correlation coefficient was calculated between genes from Arabidopsis
654 and *B. cinerea* data sets. The gene pairs with positive correlations greater than 0.74 under each
655 Arabidopsis genotype were considered to construct cross-kingdom GCNs.

656 **Dual Interaction Network Construction**

657 To construct a cross-kingdom, dual interaction network of plant-pathogen GCNs, we performed
658 principle component analysis on individual GCNs within each species to obtain eigengene
659 vectors describing the expression of the entire gene network as previously described (Zhang and
660 Horvath, 2005; Langfelder and Horvath, 2008; Okada et al., 2016). From these eigengene
661 vectors, we calculated the Spearman's rank correlation coefficient between the first eigengene
662 vectors for each network. The resulting similarity matrices were used as input to construct the
663 interaction network and Cytoscape was used to visualize the resulting network.

664 **Statistical Analysis of Network Components**

665 All the analyses were conducted using R V3.2.1 statistical environment (R Core Team, 2014). To
666 investigate how secondary metabolite induction in *B. cinerea* contributes to disease
667 development, we conducted a multi-factor ANOVA on *B. cinerea* three secondary metabolic
668 pathways upon impacts on host genotypes. The three secondary metabolic pathways included the
669 biosynthetic pathways of two well-known secondary metabolites, BOT and BOA, and a cyclic
670 peptide biosynthetic pathway predicted in this study. We calculated the z-scores for all
671 transcripts involved in BOT pathway, the BOA, and the putative cyclic peptide pathway for each
672 isolate/plant genotype pair. The multi-factor ANOVA model for lesion area was:

673 $y_{Lesion} = \mu + T * A * C * G_h + \varepsilon$

674 where T, A, C, and G_h stand for BOT, BOA, Cyclic peptide, and host genotype, respectively.

675 In addition, we used multi-factor ANOVA models to investigate interactions between GCNs
676 within species for impacts upon host genotypes. The ANOVA models contain all GCNs within a
677 species. The first eigengene vector derived from principal component analysis on each network
678 was used in ANOVA models. The ANOVA model for individual *B. cinerea* GCNs was:

679 $y_{BcNeti} = \mu + D * P * C * PSI * G_h + \varepsilon$

680 where D, P, C, PSI, and G_h stand for Arabidopsis Defense/Camalexin GCN, Arabidopsis Plastid
681 GCN, Arabidopsis Cell/Division GCN, Arabidopsis PSI GCN, and Host genotypes, respectively.
682 G_h stands for HostGenotype, respectively. BcNeti represents one of the ten *B. cinerea* GCNs
683 identified in this study. The ANOVA model for individual Arabidopsis GCNs was:

684 $y_{AtNeti} = \mu + \sum BcNeti + G_h + \varepsilon$

685 where ∑BcNeti represents the summation of each of the ten *B. cinerea* GCNs identified in this
686 study: BcVesicle/Viru GCN, BcTSL/Growth GCN, BcBOA GCN, BcExocytoRegu GCN,
687 BcCycPep GCN, BcCopperTran GCN, BcBOT GCN, BcPeptidase GCN, BcIPP GCN,
688 BcPolyketide GCN, while G_h stands for Host genotypes. Interactions among the terms were not
689 tested to avoid the potential for overfitting. AtNeti stands for one of the four Arabidopsis GCNs
690 (e.g. AtDefense/Camalexin GCN, AtPlastid GCN, AtCell/Division GCN, AtPSI GCN). All
691 multi-factor ANOVA models were optimized by trimming to just the terms with a significant *P*-
692 value (*P*-value < 0.05).

693 **Germination Assay**

694 To assess the potential for natural variation in germination time in the isolate collection, 19 *B.*
695 *cinerea* isolates were investigated by germination assay. The isolates were grown on PDA.
696 Mature spores were collected in water, filtered and resuspended in 50% grape juice, as
697 previously described, and further diluted to 1000spores/µL. To prevent germination before the
698 beginning of the assay, spores were continuously kept on ice or in the fridge at 4°C. During the
699 germination assay, the spores were maintained at 21°C in 1.5mL tubes. Every hour, the tubes
700 were mixed by manual inversion and sampled for 25µL that were transferred to microscope
701 slides. The spores within the drops were let to set down shortly. Without using slide covers, the
702 spores were observed within the drops at two locations, used as technical replicates. The spores
703 were categorized and counted based on the picture of every microscope observations taken every
704 hour from 2 to 11 hours. Germination was defined as the hyphae emerged out of the spore.

705 To assess the contribution of germination to the observed *B. cinerea* transcriptomic networks
706 involved in lesion development, we generated germination estimates based on gene expression

707 by extracting the first principal component of a publicly available time series microarray data
708 including 101 gemination-associated genes (Leroch et al., 2013). Based on this principal
709 component, we predicted the level of expression of germination-associated genes for the 96
710 isolates on the three Arabidopsis genotypes at 16HPI. Theses germination predictions for
711 individual isolates were used in a linear ANOVA model to estimate the co-linearity of the
712 germination eigengene vector to virulence. Using linear ANOVA models with and without this
713 germination eigengene vector, we compared how germination influences the 10 *B. cinerea*
714 transcriptomic networks involved in lesion area in the three host genotypes. The ANOVA
715 models with and without germination eigengene vector were:

716 $Y_{Lesion} = \mu + \text{Germination} + \sum \text{BcNeti} + G_h + \varepsilon$

717 $Y_{Lesion} = \mu + \sum \text{BcNeti} + G_h + \varepsilon$

718 where Germination represents the scores of first principal components on expressions of
719 germination associated genes from *B. cinerea* transcriptomic data in this study, ∑BcNeti
720 represents the summation of each of the ten *B. cinerea* GCNs identified in this study:
721 BcVesicle/Viru GCN, BcTSL/Growth GCN, BcBOA GCN, BcExocytoRegu GCN, BcCycPep
722 GCN, BcCopperTran GCN, BcBOT GCN, BcPeptidase GCN, BcIPP GCN, BcPolyketide GCN,
723 while G_h stands for Host genotypes. Interactions among the terms were not tested to avoid the
724 potential for overfitting.

725 **Data Availability**

726 The datasets in this study are available in the following database: Bioproject PRJNA473829
727 (https://www.ncbi.nlm.nih.gov/bioproject/?term=PRJNA473829). The computer scripts used in
728 this study are available in GitHub (https://github.com/WeiZhang317/octopus).

729 **Funding**

730 Funding for this work was provided by the NSF award IOS 1339125 to DJK, the USDA National
731 Institute of Food and Agriculture, Hatch project number CA-D-PLS-7033-H to DJK and by the
732 Danish National Research Foundation (DNRF99) grant to DJK, the China Scholarship Council
733 grant 20130624 to WZ.

734 **Figure legends**

735 **Figure 1. Correlation between earlier estimated *B. cinerea* biomass and later lesion area.**
736 Model-corrected lesion area means were estimated using the linear model on the six replicates
737 data from three Arabidopsis genotypes at 72-hours post-infection with 96 *B. cinerea* isolates.
738 Estimated biomass of *B. cinerea* was calculated using the linear model-corrected fraction of *B.*
739 *cinerea* mapped reads against total mapped reads to Arabidopsis and *B. cinerea* reference
740 genomes. RNA-Seq analysis was conducted at 16-hours post-infection for each pathosystem.
741 Three Arabidopsis genotypes are wild-type Col-0 (purple dot), jasmonate insensitive mutant
742 *coi1-1* (green triangle), and salicylic acid insensitive mutant *npr1-1* (orange diamond). The 90%
743 confidence ellipse intervals are plotted for each Arabidopsis genotype for references. Quadratic
744 regression lines are: Col-0: $y = -0.00059x^2 + 0.729x + 10.037$, $P = 0.0016$, adjusted $R^2 = 0.1101$;
745 *coi1-1*: $y = -0.117x^2 + 4.44x – 0.1585$, $P = 3.914e-07$, adjusted $R^2 = 0.2562$; *npr1-1*: $y = -$
746 $0.0579x^2 + 2.26x + 1.673$, $P = 0.0001$, adjusted $R^2 = 0.161$.

747 **Figure 2. Transcriptomic responses of *B. cinerea* on Arabidopsis are controlled by genetic**
748 **variation in pathogen population, host genotypes, and their interaction.** (A) Distribution of
749 broad-sense heritability (H^2) of *B. cinerea* transcripts contributed by genetic variation in the *B.*
750 *cinerea*, Arabidopsis genotypes, and the interaction between pathogen and host. Violin plots

751 illustrating the distribution of H^2 for transcripts from 96 *B. cinerea* isolates infecting on
752 Arabidopsis genotypes. Heritability is partitioned across the different sources, 96 pathogen
753 genotypes = "Isolate", plant genotypes Col-0, *coi1-1* and *npr1-1* plant genotypes = "Host", and
754 the corresponding interaction. The transcriptomic analysis was conducted by sequencing mRNA
755 extracted from *B. cinerea* infected Arabidopsis leaves at 16-hours post-infection. Red lines
756 indicate the average broad-sense heritability values of lesion area caused by isolates, Arabidopsis
757 genotypes, and their interaction. (B) to (E) Expression profiles of *B. cinerea* transcripts
758 significantly influenced by host genotypes. The model-corrected means ($\log_2$) for *B. cinerea*
759 transcript were used for plotting. The Arabidopsis genotypes, wild-type Col-0 (purple),
760 jasmonate insensitive mutant *coi1-1* (green), and salicylic acid mutant *npr1-1* (orange), are
761 shown on the x axis. *B. cinerea* transcripts are: (B) *Bcin01g03790.1*, class IV chitin synthase; (C)
762 *Bcin02g02980.1*, Monooxygenase; (D*) Bcin10g02260.1*, NADH oxidoreductase; (E)
763 *Bcin11g05200.1*, caffeine-induced death Cid2; (F) to (I) Expression profiles of *B. cinerea*
764 transcripts significantly influenced by the interaction between pathogen and host genotypes. (F)
765 *Bcin02g03810.1*, GTP cyclohydrolase; (G) *Bcin09g01190.1*, Tripeptidyl-peptidase 1; (H)
766 *Bcin10g01130.1*, in secretory pathway; (I) *Bcin14g05090.1*, a transcription factor.

767 **Figure 3. Expression profiles of an endopolygalacturonase gene *Bcpg1* from diverse *B.***
768 ***cinerea* isolates across Arabidopsis genotypes.** Rank plot shows the relationship of *Bcpg1*
769 expression from 32 diverse *B. cinerea* isolates (right) across three Arabidopsis genotypes (x
770 axis). Three Arabidopsis genotypes are wild-type Col-0 (purple dot), jasmonate insensitive
771 mutant *coi1-1* (green triangle), and salicylic acid mutant *npr1-1* (orange diamond). The model-
772 corrected means ($\log_2$) for the transcript of *Bcpg1* (*Bcin14g00850.1*) encoding an
773 endopolygalacturonase gene are utilized for plotting. The transcript expression levels from the

774 same isolate across three Arabidopsis genotypes are connected with a colored line. The names of
775 32 isolates are represented with the same colored lines as induced *Bcpg1* expression levels.
776 Black lines indicate the expression levels of *Bcpg1* are higher in *coi1-1* and *npr1-1* than in Col-0.
777 Red lines indicate the higher expression levels of *Bcpg1* in *coi1-1* but lower in *npr1-1*. Blue lines
778 indicate the highest expression levels of *Bcpg1* are in Col-0. Dark green lines indicate the higher
779 expression levels of *Bcpg1* in *npr1-1* but lower in *coi1-1*.

780 **Figure 4. Interaction effects of host genotypes and pathogen isolates on *B. cinerea***
781 **transcriptome.** Hierarchical clustering of relative expression of 500 genes from 96 *B. cinerea*
782 isolates infection on Arabidopsis mutants *coi1-1* (A) or *npr1-1* (B) are plotted based on pairwise
783 comparison of pathogen gene expression under Col-0. The 500 *B. cinerea* genes with highest
784 broad-sense heritability (H^2) of host X pathogen were used for analysis. Lesion area induced by
785 96 isolates are compared under *coi1-1* (orange bar plot) and npr1-1 (green bar plot).

786 **Figure 5. Gene co-expression networks identified from *B. cinerea* transcriptomic responses**
787 **to Arabidopsis wild-type Col-0 immunity.** Ten gene co-expression networks (GCNs) with
788 more than five nodes were identified from 96 *B. cinerea* isolates infecting on Arabidopsis wild-
789 type Col-0. The similarity matrix is computed using Spearman's rank correlation coefficient.
790 Nodes with different colors represent *B. cinerea* genes condensed in GCNs with different
791 biological functions. Edges represent the Spearman's rank correlation coefficients between gene
792 pairs. Trans- and cis-GCNs means GCNs are regulated by trans- and cis-regulatory elements,
793 respectively. GCNs were named after their biological functions, which were determined by hub
794 and bottleneck genes within each network. GCNs are: vesicle/virulence (red), translation/growth
795 (green), exocytosis regulation (pink), cyclic peptide (yellow), peptidase (gray), isopentenyl

796 pyrophosphate (IPP, turquoise), polyketide (violet), botcinic acid (BOA, blue), copper transport
797 (slate blue), botrydial (BOT, purple).

798 **Figure 6. Variation of transcripts accumulation for secondary metabolites production**
799 **across diverse *B. cinerea* isolates.** Expression profiles of genes responsible for botrydial,
800 botcinic acid, cyclic peptide production across 96 isolates under Arabidopsis wild-type Col-0 are
801 shown. **(**A) Schematic shows the genomic locus of seven botrydial (BOT) biosynthesis genes
802 clustered together. Exons are represented by gray boxes. Introns and intergenic regions are
803 represented by the grey line. Seven BOT genes are: *BcBOT1, BcBOT3* and *BcBOT4,* encoding a
804 cytochrome P450 monooxygenase, respectively; *BcBOT2* encoding a sesquiterpene cyclase;
805 *BcBOT5* encoding an acetyl transferase; *BcBOT6* encoding a Zn(II)2Cys6 transcription factor,
806 *BcBOT7* encoding a dehydrogenase reductase. (B) BOT biosynthesis pathway in *B. cinerea*. (C)
807 Bar plots compare expression variation of *BcBOT*2 across 96 *B. cinerea* isolates in responding to
808 Arabidopsis wild-type Col-0 immunity. The model-corrected means ($\log_2$) of transcripts were
809 used for plotting. (D) Scatter plot illustrates the positive correlations between lesion area and
810 accumulation of *BcBOT2* transcript across the 96 isolates in response to varied Arabidopsis
811 immunities. Model-corrected lesion area means were estimated for three Arabidopsis genotypes
812 at 72-hours post-infection with 96 *B. cinerea* isolates. The three Arabidopsis genotypes are
813 labeled next to the confidence ellipse curves: wild-type Col-0 (purple dot), jasmonate insensitive
814 mutant *coi1-1* (green triangle), and salicylic acid mutant *npr1-1* (orange diamond). The 90%
815 confidence ellipse intervals are plotted for each Arabidopsis genotype for reference. Linear
816 regression lines: Col-0: y = 3.2532x + 4.4323, P = 1.008e-10, Adjusted R^2 = 3.3537; *coi1-1*: y =
817 7.4802x + 10.3289, P = 7.895e-15, adjusted R^2 = 0.4700; *npr1-1*: y = 3.7086x + 7.3487, P =
818 2.425e-11, adjusted R^2 = 0.3726. (E) and (F) Bar plots compare expression variation of *BcBOA6*

819 in botcinic acid (BOA) pathway and *Bcin01g11460.* in cyclic peptide pathway across 96 *B.*
820 *cinerea* isolates in response to Arabidopsis wild-type Col-0 immunity. (G) Venn diagram
821 illustrates the number of *B. cinerea* isolates with the ability to induce BOT, BOA, and cyclic
822 peptide.

823 **Figure 7. Comparison of plasticity of *B. cinerea* gene co-expression network under vaired**
824 **host immunity.** *B. cinerea* gene co-expression networks (GCNs) of vesicle/virulence (red) and
825 translation/growth (green) identified under three Arabidopsis genotypes are compared. Three
826 Arabidopsis genotypes are wild-type Col-0, jasmonate insensitive mutant *coi1-1*, and salicylic
827 acid mutant *npr1-1*. Nodes marked with red and green colors represent *B. cinerea* genes
828 condensed in GCNs with different biological functions. The same node condensed in GCNs
829 across three Arabidopsis genotypes was marked with same color. Nodes specificaly condensed in
830 GCNs under two mutants *coi1-1* and *npr1-1* background are marked with orange color. Edges
831 represent the Spearman's rank correlation coefficients between gene pairs.

832 **Figure 8. Cross-kingdom Arabidopsis-*B. cinerea* gene co-expression networks.** Networks
833 showing the co-expression connectivity between Arabidopsis and *B. cinerea* genes within three
834 Arabidopsis genotypes are shown. (A) shows connectivity within Arabidopsis wild-type Col-0,
835 (B) shows connectivity within the Arabidopsis jasmonate insensitive mutant *coi1-1*, and (C)
836 shows connectivity within the Arabidopsis salicylic acid insensitive mutant *npr1-1*. Within each
837 connectivity plot, orange and green nodes show transcripts from *B. cinerea* and Arabidopsis,
838 respectively. Nodes with red and violet colors represent the *B. cinerea* transcripts that were
839 found to be members of the *B. cinerea* membrane/vesicle virulence network and BOT network,

840 respectively. Node size shows the number of interactions with a specific gene. The connectivity
841 between the nodes was derived using Spearman's rank correlation analysis.

842 **Figure 9. A dual interaction network reveals links between Arabidopsis immunity and *B.***
843 ***cinerea* virulence.** A dual interaction network was constructed using gene co-expression
844 networks (GCNs) from Arabidopsis and *B. cinerea* co-transcriptome. The first eigenvectors were
845 derived from individual GCNs and used as input to calculate Spearman's rank correlation
846 coefficiency between GCN pairs. Green dots and orange triangles represent Arabidopsis
847 immune- and *B. cinerea* virulence-GCNs, respectively. Blue and red lines (edges) represent the
848 positive and negative Spearman's rank correlation coefficients between GCN pairs, respectively.
849 The thickness of line signifies the correlational strength.

850 **Supplemental Data**

851 **Figure 3-figure supplemental 1**. **Expression profiles of an oxaloacetate hydrolase gene**
852 ***Bcoah* from diverse *B. cinerea* isolates across Arabidopsis genotypes.** Rank plot shows the
853 relationship o *Bcoah* expression from 32 diverse *B. cinerea* isolates (right) across three
854 Arabidopsis genotypes (x axis). Three Arabidopsis genotypes are wild-type Col-0 (purple dot),
855 jasmonate insensitive mutant *coi1-1* (green triangle), and salicylic acid mutant *npr1-1* (orange
856 diamond). The model-corrected means ($\log_2$) for the transcript of *Bcoah* (*Bcin12g01020.1*)
857 encoding an oxaloacetate hydrolase gene are utilized for plotting. The transcript expression
858 levels from the same isolate across three Arabidopsis genotypes are connected with a colored
859 line. The names of 32 isolates are represented with the same colored lines as induced *Bcoah*
860 expression levels. Black lines indicate the expression levels of *Bcoah* are higher in *coi1-1* and
861 *npr1-1* than in Col-0. Red lines indicate the higher expression levels of *Bcoah* in *coi1-1* but

862 lower in *npr1-1*. Blue lines indicate the highest expression levels of *Bcoah* are in Col-0. Dark
863 green lines indicate the higher expression levels of *Bcoah* in *npr1-1* but lower in *coi1-1*.

864 **Figure 5-figure supplemental 1. Genomic location of *B. cinerea* gene co-expression**
865 **networks.** The circle diagrams showed the genome-wide distribution of gene pairs identified by
866 *B. cinerea* gene co-expression networks (GCNs) under Arabidopsis wild-type Col-0. (A) to (J)
867 Genomic locations of gene pairs identified by GCNs: (A) Vesicle/virulence, (B)
868 translation/growth, (C) botcinic acid (BOA), (D) exocytosis regulation, (E) cyclic peptide, (F)
869 copper transport, (G) botrydial (BOT), (H) peptidase (gray), (I) isopentenyl pyrophosphate (IPP),
870 (G) polyketide. The rings show 18 *B. cinerea* chromosomes on a Mb scale. Genomic locations of
871 co-expressed gene pairs are connected by the colored lines.

872 **Figure 7-figure supplemental 1. Gene co-expression networks identified from *B. cinerea***
873 **transcriptomic responses to Arabidopsis wild-type Col-0 immunity.** *B. cinerea* gene co-
874 expression networks (GCNs) were identified from 96 *B. cinerea* isolates infecting on
875 Arabidopsis wild-type Col-0. The similarity matrix is computed using Spearman's rank
876 correlation coefficient. All co-expressed gene pairs with correlation greater than 0.85 were
877 shown. Nodes with different colors represent *B. cinerea* genes condensed in GCNs with different
878 biological functions. Edges represent the Spearman's rank correlation coefficients between gene
879 pairs. GCNs were ordered as number of nodes within each network. GCNs were named after
880 their biological functions, which were determined by hub and bottleneck genes within each
881 network: vesicle/virulence (red), translation/growth (green), botcinic acid (BOA, blue),
882 exocytosis regulation (pink), cyclic peptide (yellow), copper transport (slate blue), botrydial
883 (BOT, purple), peptidase (gray), isopentenyl pyrophosphate (IPP, turquoise), polyketide (violet).

884 **Figure 7-figure supplemental 2. Gene co-expression networks identified from *B. cinerea***
885 **transcriptomic responses to Arabidopsis jasmonate-compromised immunity.** *B. cinerea*
886 gene co-expression networks (GCNs) were identified from 96 *B. cinerea* isolates infecting on
887 Arabidopsis jasmonate insensitive mutant *coi1-1*. The similarity matrix is computed using
888 Spearman's rank correlation coefficient. All co-expressed gene pairs with correlation greater
889 than 0.8 were shown. Nodes with different colors represent *B. cinerea* genes condensed in GCNs
890 with different biological functions. Nodes were marked with same color as under Arabidopsis
891 wild-type Col-0 background. Nodes specificaly condenced in GCNs under Arabidopsis mutant
892 *coi1-1* background are marked with orange color. Edges represent the Spearman's rank
893 correlation coefficients between gene pairs. GCNs were ordered as number of nodes within each
894 network. GCNs were named after their biological functions, which were determined by hub and
895 bottleneck genes within each network: vesicle/virulence (red/orange), translation/growth
896 (green/orange), botrydial/ isopentenyl pyrophosphate (BOT/IPP, blue/turquoise/orange), botcinic
897 acid (BOA, blue), exocytosis regulation (pink), peptidase (gray/orange), copper transport (slate
898 blue/orange), plant cell wall degradation (orange), cyclic peptide (yellow), peptidase II
899 (red/orange), siderophores (orange), 26S proteasome regulated protein degradation (red/orange),
900 sugar, ROS/NO stress (orange), ATP (orange), polyketide (violet/orange).

901 **Figure 7-figure supplemental 3. Gene co-expression networks identified from *B. cinerea***
902 **transcriptomic responses to Arabidopsis salicylic acid-compromised immunity.** *B. cinerea*
903 gene co-expression networks (GCNs) were identified from 96 *B. cinerea* isolates infecting on
904 Arabidopsis salicylic acid insensitive mutant *npr1-1*. The similarity matrix is computed using
905 Spearman's rank correlation coefficient. All co-expressed gene pairs with correlation greater
906 than 0.8 were shown. Nodes with different colors represent *B. cinerea* genes condensed in GCNs

907 with different biological functions. Nodes were marked with same color as under Arabidopsis
908 wild-type Col-0 background. Nodes specificaly condenced in GCNs under Arabidopsis mutant
909 *npr1-1* background are marked with orange color. Edges represent the Spearman's rank
910 correlation coefficients between gene pairs. GCNs were ordered as number of nodes within each
911 network. GCNs were named after their biological functions, which were determined by hub and
912 bottleneck genes within each network: translation/growth (green/orange), vesicle/virulence
913 (red/orange), peptidase (gray/orange), polyketide (violet/orange), botrydial/isopentenyl
914 pyrophosphate (BOT/IPP, blue/turquoise/orange), botcinic acid (BOA, blue), exocytosis
915 regulation (pink), copper transport (slate blue/orange), cyclic peptide (yellow), unknown (red),
916 sugar (orange), peptidase II (red/orange).

917 **Figure 7-figure supplemental 4. Plasticity in expression profiles of genes identified by *B.***
918 ***cinerea* gene co-expression networks under varied Arabidopsis immunities.** Violin plots of
919 (A) to (O) show the expression profiles of *B. cinerea* genes in response to variation of
920 Arabidopsis immunity. Genes shown are condensed in *B. cinerea* gene co-expression networks
921 (GCNs). The model-corrected means ($\log_2$) for *B. cinerea* transcript were used for plotting. The
922 Arabidopsis genotypes, wild-type Col-0 (purple), jasmonate insensitive mutant *coi1-1* (green),
923 and salicylic acid mutant *npr1-1* (orange), are shown on the x axis.

924 **Figure 8-figure supplemental 1. Associations between gene co-expression networks**
925 **identified from co- and single-transcriptome.** Venn diagrams highlights: (A) the overlap of
926 plant (left) and pathogen (right) genes condensed in Arabidopsis-*B. cinerea* gene co-expression
927 networks (GCNs) across three Arabidopsis genotypes, (B) the overlap of plant genes in

928 Arabidopsis-B. cinerea GCNs and Arabidopsis GCNs across three genotypes, (C) the overlap of
929 pathogen genes in Arabidopsis-*B. cinerea* GCNs and *B. cinerea* GCNs across three genotypes.

930 **Figure 9-figure supplemental 1. Dual networks reveal links between Arabidopsis immunity**
931 **and *B. cinerea* virulence under *coi1-1* and *npr1-1*.** Dual interaction networks were constructed
932 using gene co-expression networks (GCNs) from Arabidopsis and *B. cinerea* co-transcriptome
933 under JA-insensitive mutant *coi1-1* and SA-insensitive mutant *npr1-1*, respectively. The first
934 eigenvectors were derived from individual GCNs and used as input to calculate Spearman's rank
935 correlation coefficiency between GCN pairs. Green dots and orange triangles (nodes) represent
936 Arabidopsis immune- and *B. cinerea* virulence-GCNs, respectively. Blue and red lines (edges)
937 represent the positive and negative Spearman's rank correlation coefficients between GCN pairs,
938 respectively. The thickness of line signifies the correlational strength.

939 **Figure 9-figure supplemental 2. Variation of *B. cinerea* spore germination time under *in***
940 ***vitro* condition.**

941 **Supplemental Table 1. Topology traits of *B. cinerea in planta* gene co-expression networks.**

942 **Supplemental Table 2. ANOVA table of lesion area and *B. cinerea* pathways.** A mixed linear
943 model was fitted to test lesion area and *B. cinerea* pathways responsible for botrydial (BOT),
944 botcinic acid (BOA), and cyclic peptide (CycPep) produced under three Arabidopsis genotypes.
945 The lesion area data used in the model were GLM corrected least square means induced by 96 *B.*
946 *cinerea* isolates. Model-corrected means of transcripts from 96 *B. cinerea* isolates were z-scaled
947 and used in ANOVA. Df is the degrees of freedom for a term within the model. SS is the Sum of
948 Squares variation. MS is the Mean of Squared variation. F value is derived from the F statistic

949 and *P*-value indicates the statistical significance for a given term within the model. Significance
950 of differences are shown as $P < 0.001$ '***', 0.01'**' and 0.05 '*'.

951 **Supplemental Table 3. ANOVA tables of *B. cinerea* gene co-expression networks. Mixed**
952 linear models were fitted to individual *B. cinerea* (Bc) gene co-expression networks (GCNs) and
953 variation of host genotypes and Arabidopsis (At) GCNs. Variation was estimated among host
954 genotypes and first eigenvectors from four individual Arabidopsis GCNs. Df is the degrees of
955 freedom for a term within the model. SS is the Sum of Squares variation. MS is the Mean of
956 Squared variation. F value is derived from the F statistic and *P*-value indicates the statistical
957 significance for a given term within the model. Significance of difference are shown as $P < 0.001$
958 '***', 0.01'**' and 0.05 '*'.

959 **Supplemental Table 4**. **ANOVA tables of Arabidopsis gene co-expression networks.** Linear
960 mixed models were fitted to individual Arabidopsis (At) gene co-expression networks (GCNs)
961 and variation of host genotypes and ten *B. cinerea* (Bc) GCNs. Variation was estimated among
962 host genotypes and first eigenvectors from individual *B. cinerea* GCNs. Df is the degrees of
963 freedom for a term within the model. SS is the Sum of Squares variation. MS is the Mean of
964 Squared variation. F value is derived from the F statistic and *P*-value indicates the statistical
965 significance for a given term within the model. Significance of difference are shown as $P < 0.001$
966 '***', 0.01'**' and 0.05 '*'.

967 **Supplemental Table 5. Topology traits of cross-kingdom Arabidopsis-*B. cinerea* gene co-**
968 **expression networks.** Three Arabidopsis genotypes are wild-type Col-0, jasmonate insensitive
969 mutant *coi1-1*, and salicylic acid insensitive mutant *npr1-1*.

970 **Supplemental Table 6. Analysis of potential impact of germination variation.** To test if
971 germination may influence the observed network to lesion connections, we estimated
972 germination using the first principal component of genes linked to germination in Leroch et al.,
973 2013. We then estimated the value of this principal component in the isolates grown on the three
974 host genotypes and conducted a linear model to compare how this eigengene links to virulence.
975 Using a linear model with and without this germination eigengene, we compared the link of the
976 10 *B. cinerea* transcript networks to lesion size with and without the germination eigengene
977 vector in the model.

978 **Supplemental Data Set 1. Model-corrected means of *B. cinerea* transcripts.** A table of
979 model-corrected least-square means of *B. cinerea* transcripts from 96 isolates infection on
980 Arabidopsis wild-type Col-0, jasmonate insensitive mutant *coi1-1*, and salicylic acid insensitive
981 mutant *npr1-1*.

982 **Supplemental Data Set 2. Standard errors of *B. cinerea* transcripts.** A table of model-
983 corrected standard errors of *B. cinerea* transcripts infection on Arabidopsis wild-type Col-0,
984 jasmonate insensitive mutant *coi1-1*, and salicylic acid insensitive mutant *npr1-1*.

985 **Supplemental Data Set 3. GLM deviance tables and broad-sense heritability of *B. cinerea***
986 **transcripts.** Summary of deviance tables derived from generalized linear model and estimated
987 broad-sense heritability (H^2) for *B. cinerea* transcripts. All significance values are corrected by
988 false discovery rate.

989 **Supplemental Data Set 4. Model-corrected means of estimated *B. cinerea* biomass.** *B.*
990 *cinerea* biomass of 96 isolates infection on Arabidopsis genotypes was estimated using the

991 fraction of uniquely mapped reads against B05.10 reference genome. Three Arabidopsis
992 genotypes are wild-type Col-0, jasmonate insensitive mutant *coi1-1*, and salicylic acid
993 insensitive mutant *npr1-1*.

994 **Supplemental Data Set 5. Top 100 heritability of *B. cinerea* transcripts.** Broad-sense
995 heritability (H^2) of individual *B. cinerea* transcript contributed by pathogen, host and their
996 interaction were estimated. Three Arabidopsis genotypes are wild-type Col-0, jasmonate
997 insensitive mutant *coi1-1*, and salicylic acid insensitive mutant *npr1-1*.

998 **Supplemental Data Set 6. Spearman's rank correlation between lesion area and *B. cinerea***
999 **transcripts abundance.** A table of spearman's rank correlation coefficiency between lesion area
1000 and *B. cinerea* transcripts accumulation across three Arabidopsis genotypes or under individual
1001 genotypes. Three Arabidopsis genotypes are wild-type Col-0, jasmonate insensitive mutant *coi1-*
1002 *1*, and salicylic acid insensitive mutant *npr1-1*.

1003 **Supplemental Data Set 7. Gene list of *B. cinerea* gene co-expression networks.** Tables of *B.*
1004 *cinerea* genes identified by *B. cinerea* gene co-expression networks (GCNs) during 96 isolates
1005 infection on Arabidopsis wild-type Col-0, jasmonate insensitive mutant *coi1-1*, and salicylic acid
1006 insensitive mutant *npr1-1*.

1007 **Supplemental Data Set 8. Gene list of cross-kingdom Arabidopsis-*B. cinerea* gene co-**
1008 **expression networks.** Tables of Arabidopsis and *B. cinerea* genes identified by co-transcriptome
1009 gene co-expression networks (GCNs) during 96 isolates infection on Arabidopsis wild-type Col-
1010 0, jasmonate insensitive mutant *coi1-1*, and salicylic acid insensitive mutant *npr1-1*.

1011 **References**

1012 **Arbelet, D., Malfatti, P., Simond-Cote, E., Fontaine, T., Desquilbet, L., Expert, D., Kunz,**
1013 **C., and Soulie, M.C.** (2010). Disruption of the Bcchs3a chitin synthase gene in Botrytis cinerea
1014 is responsible for altered adhesion and overstimulation of host plant immunity. Mol. Plant
1015 Microbe Interact. **23,** 1324-1334, doi/10.1094/MPMI-02-10-0046.

1016 **Ascari, J., Boaventura, M.A., Takahashi, J.A., Duran-Patron, R., Hernandez-Galan, R.,**
1017 **Macias-Sanchez, A.J., and Collado, I.G.** (2013). Phytotoxic activity and metabolism of
1018 Botrytis cinerea and structure-activity relationships of isocaryolane derivatives. J. Nat. Prod. **76,**
1019 1016-1024, doi/10.1021/np3009013.

1020 **Atwell, S., Corwin, J.A., Soltis, N.E., Subedy, A., Denby, K.J., and Kliebenstein, D.J.**
1021 (2015). Whole genome resequencing of Botrytis cinerea isolates identifies high levels of
1022 standing diversity. Front. Microbiol. **6,** 996, doi/10.3389/fmicb.2015.00996.

1023 **Bednarek, P., Pislewska-Bednarek, M., Svatos, A., Schneider, B., Doubsky, J., Mansurova,**
1024 **M., Humphry, M., Consonni, C., Panstruga, R., Sanchez-Vallet, A., Molina, A., and**
1025 **Schulze-Lefert, P.** (2009). A glucosinolate metabolism pathway in living plant cells mediates
1026 broad-spectrum antifungal defense. Science **323,** 101-106, doi/10.1126/science.1163732.

1027 **Benjamini Yoav and Yekutieli Daniel** (2001). The Control of the False Discovery Rate in
1028 Multiple Testing under Dependency. **29,** 1165-1188, doi/10.1214/aos/1013699998.

1029 **Benton, M.J.** (2009). The Red Queen and the Court Jester: species diversity and the role of
1030 biotic and abiotic factors through time. Science **323,** 728-732, doi/10.1126/science.1157719.

1031 **Bergelson, J., Kreitman, M., Stahl, E.A., and Tian, D.** (2001). Evolutionary dynamics of plant
1032 R-genes. Science **292,** 2281-2285, doi/10.1126/science.1061337.

1033 **Blanco-Ulate, B., Morales-Cruz, A., Amrine, K.C., Labavitch, J.M., Powell, A.L., and**
1034 **Cantu, D.** (2014). Genome-wide transcriptional profiling of Botrytis cinerea genes targeting
1035 plant cell walls during infections of different hosts. Front. Plant. Sci. **5,** 435,
1036 doi/10.3389/fpls.2014.00435.

1037 **Brooks, D.M., Bender, C.L., and Kunkel, B.N.** (2005). The Pseudomonas syringae phytotoxin
1038 coronatine promotes virulence by overcoming salicylic acid-dependent defences in Arabidopsis
1039 thaliana. Mol. Plant. Pathol. **6,** 629-639, doi/10.1111/j.1364-3703.2005.00311.x.

1040 **Bullard, J.H., Purdom, E., Hansen, K.D., and Dudoit, S.** (2010). Evaluation of statistical
1041 methods for normalization and differential expression in mRNA-Seq experiments. BMC
1042 Bioinformatics **11,** 94, doi/10.1186/1471-2105-11-94.

1043 **Buttner, D. and He, S.Y.** (2009). Type III protein secretion in plant pathogenic bacteria. Plant
1044 Physiol. **150,** 1656-1664, doi/10.1104/pp.109.139089.

1045 **Cantarel, B.L., Coutinho, P.M., Rancurel, C., Bernard, T., Lombard, V., and Henrissat, B.**
1046 (2009). The Carbohydrate-Active EnZymes database (CAZy): an expert resource for
1047 Glycogenomics. **37,** D233–D238, doi/10.1093/nar/gkn663.

1048 **Cao, H., Glazebrook, J., Clarke, J.D., Volko, S., and Dong, X.** (1997). The Arabidopsis NPR1
1049 gene that controls systemic acquired resistance encodes a novel protein containing ankyrin
1050 repeats. Cell **88,** 57-63, doi/10.1016/S0092-8674(00)81858-9.

1051 **Choquer, M., Fournier, E., Kunz, C., Levis, C., Pradier, J.M., Simon, A., and Viaud, M.**
1052 (2007). Botrytis cinerea virulence factors: new insights into a necrotrophic and polyphageous
1053 pathogen. FEMS Microbiol. Lett. **277,** 1-10, doi/10.1111/j.1574-6968.2007.00930.x.

1054 **Clay, N.K., Adio, A.M., Denoux, C., Jander, G., and Ausubel, F.M.** (2009). Glucosinolate
1055 metabolites required for an Arabidopsis innate immune response. Science **323,** 95-101,
1056 doi/10.1126/science.1164627.

1057 **Colmenares, A.J., Aleu, J., Duran-Patron, R., Collado, I.G., and Hernandez-Galan, R.**
1058 (2002). The putative role of botrydial and related metabolites in the infection mechanism of
1059 Botrytis cinerea. J. Chem. Ecol. **28,** 997-1005, doi/1015209817830.

1060 **Colombo, M., Raposo, G., and Thery, C.** (2014). Biogenesis, secretion, and intercellular
1061 interactions of exosomes and other extracellular vesicles. Annu. Rev. Cell Dev. Biol. **30,** 255-
1062 289, doi/10.1146/annurev-cellbio-101512-122326.

1063 **Conesa, A., Gotz, S., Garcia-Gomez, J.M., Terol, J., Talon, M., and Robles, M.** (2005).
1064 Blast2GO: a universal tool for annotation, visualization and analysis in functional genomics
1065 research. Bioinformatics **21,** 3674-3676, doi/10.1093/bioinformatics/bti610.

1066 **Corwin, J.A., Copeland, D., Feusier, J., Subedy, A., Eshbaugh, R., Palmer, C., Maloof, J.,**
1067 **and Kliebenstein, D.J.** (2016). The Quantitative Basis of the Arabidopsis Innate Immune
1068 System to Endemic Pathogens Depends on Pathogen Genetics. PLoS Genet. **12,** e1005789,
1069 doi/10.1371/journal.pgen.1005789.

1070 **Corwin, J.A., Subedy, A., Eshbaugh, R., and Kliebenstein, D.J.** (2016). Expansive
1071 Phenotypic Landscape of Botrytis cinerea Shows Differential Contribution of Genetic Diversity
1072 and Plasticity. Mol. Plant Microbe Interact. **29,** 287-298, doi/10.1094/MPMI-09-15-0196-R.

1073 **Corwin, J.A. and Kliebenstein, D.J.** (2017). Quantitative Resistance: More Than Just
1074 Perception of a Pathogen. Plant Cell **29,** 655-665, doi/10.1105/tpc.16.00915.

1075 **Courtade, G., Wimmer, R., Røhr, ÅK., Preims, M., Felice, A.K.G., Dimarogona, M., Vaaje-**
1076 **Kolstad, G., Sørlie, M., Sandgren, M., Ludwig, R., Eijsink, V.G.H., and Aachmann, F.L.**
1077 (2016). Interactions of a fungal lytic polysaccharide monooxygenase with β-glucan substrates
1078 and cellobiose dehydrogenase. **113,** 5922, doi/10.1073/pnas.1602566113.

1079 **Couto, D. and Zipfel, C.** (2016). Regulation of pattern recognition receptor signalling in plants.
1080 Nat. Rev. Immunol. **16,** 537-552, doi/10.1038/nri.2016.77.

1081 **Cui, H., Qiu, J., Zhou, Y., Bhandari, D.D., Zhao, C., Bautor, J., and Parker, J.E.** (2018).
1082 Antagonism of Transcription Factor MYC2 by EDS1/PAD4 Complexes Bolsters Salicylic Acid
1083 Defense in Arabidopsis Effector-Triggered Immunity. Mol. Plant. **11,** 1053-1066,
1084 doi/10.1016/j.molp.2018.05.007.

1085 **Dalmais, B., Schumacher, J., Moraga, J., LE Pêcheur, P., Tudzynski, B., Collado, I.G., and**
1086 **Viaud, M.** (2011). The Botrytis cinerea phytotoxin botcinic acid requires two polyketide
1087 synthases for production and has a redundant role in virulence with botrydial. **12,** 564,
1088 doi/10.1111/j.1364-3703.2010.00692.x.

1089 **Dangl, J.L. and Jones, J.D.** (2001). Plant pathogens and integrated defence responses to
1090 infection. Nature **411,** 826-833, doi/10.1038/35081161.

1091 **Deighton, N., Muckenschnabel, I., Colmenares, A.J., Collado, I.G., and Williamson, B.**
1092 (2001). Botrydial is produced in plant tissues infected by Botrytis cinerea. Phytochemistry **57,**
1093 689-692, doi/10.1016/S0031-9422(01)00088-7.

1094 **Denby, K.J., Kumar, P., and Kliebenstein, D.J.** (2004). Identification of Botrytis cinerea
1095 susceptibility loci in Arabidopsis thaliana. Plant J. **38,** 473-486, doi/10.1111/j.0960-
1096 7412.2004.02059.x.

1097 **Ding Qiong and Zhang Jinlong** (2012). seqRFLP: Simulation and visualization of restriction
1098 enzyme cutting pattern from DNA sequences. **R package version 1.0.1.,** .

1099 **Fordyce, R.F., Soltis, N.E., Caseys, C., Gwinner, R., Corwin, J.A., Atwell, S., Copeland, D.,**
1100 **Feusier, J., Subedy, A., Eshbaugh, R., and Kliebenstein, D.J.** (2018). Digital Imaging
1101 Combined with Genome-Wide Association Mapping Links Loci to Plant-Pathogen Interaction
1102 Traits. Plant Physiol., doi/10.1104/pp.18.00851.

1103 **Fox, J. and Weisberg, S.** (2011). An R Companion to Applied Regression, Second Edition ed.
1104 (Sage, CA: Thousand Oaks).

1105 **Frerigmann, H., Pislewska-Bednarek, M., Sanchez-Vallet, A., Molina, A., Glawischnig, E.,**
1106 **Gigolashvili, T., and Bednarek, P.** (2016). Regulation of Pathogen-Triggered Tryptophan
1107 Metabolism in Arabidopsis thaliana by MYB Transcription Factors and Indole Glucosinolate
1108 Conversion Products. Mol. Plant. **9,** 682-695, doi/10.1016/j.molp.2016.01.006.

1109 **Gerbi, C., Bata, J., Breton, A., and Prensier, G.** (1996). Glycoside and polysaccharide
1110 hydrolase activity of the rumen anaerobic fungus Caecomyces communis (Sphaeromonas
1111 communis SENSU ORPIN) at early and final stages of the developmental cycle. Curr. Microbiol.
1112 **32,** 256-259, doi/10.1007/s002849900046.

1113 **Glazebrook, J.** (2005). Contrasting mechanisms of defense against biotrophic and necrotrophic
1114 pathogens. Annu. Rev. Phytopathol. **43,** 205-227, doi/10.1146/annurev.phyto.43.040204.135923.

1115 **Gotz, S., Garcia-Gomez, J.M., Terol, J., Williams, T.D., Nagaraj, S.H., Nueda, M.J.,**
1116 **Robles, M., Talon, M., Dopazo, J., and Conesa, A.** (2008). High-throughput functional
1117 annotation and data mining with the Blast2GO suite. Nucleic Acids Res. **36,** 3420-3435,
1118 doi/10.1093/nar/gkn176.

1119 **Govrin, E.M. and Levine, A.** (2000). The hypersensitive response facilitates plant infection by
1120 the necrotrophic pathogen Botrytis cinerea. Curr. Biol. **10,** 751-757, doi/10.1016/S0960-
1121 9822(00)00560-1.

1122 **Greenberg, J.T., Guo, A., Klessig, D.F., and Ausubel, F.M.** (1994). Programmed cell death in
1123 plants: a pathogen-triggered response activated coordinately with multiple defense functions.
1124 Cell **77,** 551-563, doi/10.1016/0092-8674(94)90217-8.

1125 **Igarashi, K., Uchihashi, T., Uchiyama, T., Sugimoto, H., Wada, M., Suzuki, K., Sakuda, S.,**
1126 **Ando, T., Watanabe, T., and Samejima, M.** (2014). Two-way traffic of glycoside hydrolase
1127 family 18 processive chitinases on crystalline chitin. Nat. Commun. **5,** 3975,
1128 doi/10.1038/ncomms4975.

1129 **Ingo Morgenstern, Justin Powlowski, and Adrian Tsang** (2014). Fungal cellulose degradation
1130 by oxidative enzymes: from dysfunctional GH61 family to powerful lytic polysaccharide
1131 monooxygenase family. **13,** 471, doi/10.1093/bfgp/elu032.

1132 **Jones, J.D. and Dangl, J.L.** (2006). The plant immune system. Nature **444,** 323-329,
1133 doi/10.1038/nature05286.

1134 **Kanzaki, H., Yoshida, K., Saitoh, H., Fujisaki, K., Hirabuchi, A., Alaux, L., Fournier, E.,**
1135 **Tharreau, D., and Terauchi, R.** (2012). Arms race co-evolution of Magnaporthe oryzae AVR-
1136 Pik and rice Pik genes driven by their physical interactions. Plant J. **72,** 894-907,
1137 doi/10.1111/j.1365-313X.2012.05110.x.

1138 **Karasov, T.L., Kniskern, J.M., Gao, L., DeYoung, B.J., Ding, J., Dubiella, U., Lastra, R.O.,**
1139 **Nallu, S., Roux, F., Innes, R.W., Barrett, L.G., Hudson, R.R., and Bergelson, J.** (2014). The
1140 long-term maintenance of a resistance polymorphism through diffuse interactions. Nature **512,**
1141 436-440, doi/10.1038/nature13439.

1142 **Kliebenstein, D.J., Rowe, H.C., and Denby, K.J.** (2005). Secondary metabolites influence
1143 Arabidopsis/Botrytis interactions: variation in host production and pathogen sensitivity. Plant J.
1144 **44,** 25-36, doi/10.1111/j.1365-313X.2005.02508.x.

1145 **Krishnakumar, V., Hanlon, M.R., Contrino, S., Ferlanti, E.S., Karamycheva, S., Kim, M.,**
1146 **Rosen, B.D., Cheng, C.Y., Moreira, W., Mock, S.A., Stubbs, J., Sullivan, J.M., Krampis, K.,**
1147 **Miller, J.R., Micklem, G., Vaughn, M., and Town, C.D.** (2015). Araport: the Arabidopsis
1148 information portal. Nucleic Acids Res. **43,** 1003, doi/10.1093/nar/gku1200.

1149 **Kubicek, C.P., Starr, T.L., and Glass, N.L.** (2014). Plant cell wall-degrading enzymes and
1150 their secretion in plant-pathogenic fungi. Annu. Rev. Phytopathol. **52,** 427-451,
1151 doi/10.1146/annurev-phyto-102313-045831.

1152 **Kumar, R., Ichihashi, Y., Kimura, S., Chitwood, D.H., Headland, L.R., Peng, J., Maloof,**
1153 **J.N., and Sinha, N.R.** (2012). A High-Throughput Method for Illumina RNA-Seq Library
1154 Preparation. Front. Plant. Sci. **3,** 202, doi/10.3389/fpls.2012.00202.

1155 **Lamesch, P., Dreher, K., Swarbreck, D., Sasidharan, R., Reiser, L., and Huala, E.** (2010).
1156 Using the Arabidopsis information resource (TAIR) to find information about Arabidopsis genes.
1157 Curr. Protoc. Bioinformatics **Chapter 1,** Unit1.11, doi/10.1002/cpbi.36.

1158 **Lamesch, P., Berardini, T.Z., Li, D., Swarbreck, D., Wilks, C., Sasidharan, R., Muller, R.,**
1159 **Dreher, K., Alexander, D.L., Garcia-Hernandez, M., Karthikeyan, A.S., Lee, C.H., Nelson,**
1160 **W.D., Ploetz, L., Singh, S., Wensel, A., and Huala, E.** (2012). The Arabidopsis Information
1161 Resource (TAIR): improved gene annotation and new tools. Nucleic Acids Res. **40,** 1202,
1162 doi/10.1093/nar/gkr1090.

1163 **Langfelder, P. and Horvath, S.** (2008). WGCNA: an R package for weighted correlation
1164 network analysis. BMC Bioinformatics **9,** 559, doi/10.1186/1471-2105-9-559.

1165 **Langmead, B., Trapnell, C., Pop, M., and Salzberg, S.L.** (2009). Ultrafast and memory-
1166 efficient alignment of short DNA sequences to the human genome. Genome Biol. **10,** r25. Epub
1167 2009 Mar 4, doi/10.1186/gb-2009-10-3-r25.

1168 **Lanver, D., Muller, A.N., Happel, P., Schweizer, G., Haas, F.B., Franitza, M., Pellegrin, C.,**
1169 **Reissmann, S., Altmuller, J., Rensing, S.A., and Kahmann, R.** (2018). The Biotrophic
1170 Development of Ustilago maydis Studied by RNA-Seq Analysis. Plant Cell **30,** 300-323,
1171 doi/10.1105/tpc.17.00764.

1172 **Lee, H.J., Georgiadou, A., Walther, M., Nwakanma, D., Stewart, L.B., Levin, M., Otto,**
1173 **T.D., Conway, D.J., Coin, L.J., and Cunnington, A.J.** (2018). Integrated pathogen load and
1174 dual transcriptome analysis of systemic host-pathogen interactions in severe malaria. Sci. Transl.
1175 Med. **10,** 10.1126/scitranslmed.aar3619, doi/10.1126/scitranslmed.aar3619.

1176 **Leroch, M., Kleber, A., Silva, E., Coenen, T., Koppenhofer, D., Shmaryahu, A., Valenzuela,**
1177 **P.D., and Hahn, M.** (2013). Transcriptome profiling of Botrytis cinerea conidial germination
1178 reveals upregulation of infection-related genes during the prepenetration stage. Eukaryot. Cell.
1179 **12,** 614-626, doi/10.1128/EC.00295-12 [doi].

1180 **Li, H., Handsaker, B., Wysoker, A., Fennell, T., Ruan, J., Homer, N., Marth, G., Abecasis,**
1181 **G., Durbin, R., and 1000 Genome Project Data Processing Subgroup** (2009). The Sequence
1182 Alignment/Map format and SAMtools. Bioinformatics **25,** 2078-2079,
1183 doi/10.1093/bioinformatics/btp352.

1184 **Macheleidt, J., Mattern, D.J., Fischer, J., Netzker, T., Weber, J., Schroeckh, V., Valiante,**
1185 **V., and Brakhage, A.A.** (2016). Regulation and Role of Fungal Secondary Metabolites. Annu.
1186 Rev. Genet. **50,** 371-392, doi/10.1146/annurev-genet-120215-035203.

1187 **McClure, R.S., Overall, C.C., Hill, E.A., Song, H.S., Charania, M., Bernstein, H.C.,**
1188 **McDermott, J.E., and Beliaev, A.S.** (2018). Species-specific transcriptomic network inference
1189 of interspecies interactions. ISME J. **12,** 2011-2023, doi/10.1038/s41396-018-0145-6.

1190 **Mengiste, T., Chen, X., Salmeron, J., and Dietrich, R.** (2003). The BOTRYTIS
1191 SUSCEPTIBLE1 gene encodes an R2R3MYB transcription factor protein that is required for
1192 biotic and abiotic stress responses in Arabidopsis. Plant Cell **15,** 2551-2565,
1193 doi/10.1105/tpc.014167.

1194 **Mengiste, T.** (2012). Plant immunity to necrotrophs. Annu. Rev. Phytopathol. **50,** 267-294,
1195 doi/10.1146/annurev-phyto-081211-172955.

1196 **Mine, A., Seyfferth, C., Kracher, B., Berens, M.L., Becker, D., and Tsuda, K.** (2018). The
1197 Defense Phytohormone Signaling Network Enables Rapid, High-Amplitude Transcriptional
1198 Reprogramming during Effector-Triggered Immunity. Plant Cell **30,** 1199-1219,
1199 doi/10.1105/tpc.17.00970.

1200 **Mittal, S. and Davis, K.R.** (1995). Role of the phytotoxin coronatine in the infection of
1201 Arabidopsis thaliana by Pseudomonas syringae pv. tomato. Mol. Plant Microbe Interact. **8,** 165-
1202 171.

1203 **Moraga, J., Dalmais, B., Izquierdo-Bueno, I., Aleu, J., Hanson, J.R., Hernandez-Galan, R.,**
1204 **Viaud, M., and Collado, I.G.** (2016). Genetic and Molecular Basis of Botrydial Biosynthesis:
1205 Connecting Cytochrome P450-Encoding Genes to Biosynthetic Intermediates. ACS Chem. Biol.
1206 **11,** 2838-2846, doi/10.1021/acschembio.6b00581.

1207 **Movahedi, S., Norey, C.G., Kay, J., and Heale, J.B.** (1991). Infection and pathogenesis of cash
1208 crops by Botrytis cinerea: primary role of an aspartic proteinase. **306,** 213.

1209 **Musungu, B.M., Bhatnagar, D., Brown, R.L., Payne, G.A., OBrian, G., Fakhoury, A.M.,**
1210 **and Geisler, M.** (2016). A Network Approach of Gene Co-expression in the Zea
1211 mays/Aspergillus flavus Pathosystem to Map Host/Pathogen Interaction Pathways. Front. Genet.
1212 **7,** 206, doi/10.3389/fgene.2016.00206.

1213 **Nelson, C.E., Attia, M.A., Rogowski, A., Morland, C., Brumer, H., and Gardner, J.G.**
1214 (2017). Comprehensive functional characterization of the glycoside hydrolase family 3 enzymes
1215 from Cellvibrio japonicus reveals unique metabolic roles in biomass saccharification. Environ.
1216 Microbiol. **19,** 5025-5039, doi/10.1111/1462-2920.13959.

1217 **Nobori, T., Velasquez, A.C., Wu, J., Kvitko, B.H., Kremer, J.M., Wang, Y., He, S.Y., and**
1218 **Tsuda, K.** (2018). Transcriptome landscape of a bacterial pathogen under plant immunity. Proc.
1219 Natl. Acad. Sci. U. S. A. **115,** E3064, doi/10.1073/pnas.1800529115.

1220 **Okada, H., Ebhardt, H.A., Vonesch, S.C., Aebersold, R., and Hafen, E.** (2016). Proteome-
1221 wide association studies identify biochemical modules associated with a wing-size phenotype in
1222 Drosophila melanogaster. Nat. Commun. **7,** 12649, doi/10.1038/ncomms12649.

1223 **Pages, H., Aboyoun, P., Gentleman, R., and DebRoy, S.** (2017). Biostrings: String objects
1224 representing biological sequences, and matching algorithms. **R package version 2.44.2.,** .

1225 **Pérez-Izquierdo, L., Morin, E., Maurice, J.P., Martin, F., Rincón, A., and Buée, M.** (2017).
1226 A new promising phylogenetic marker to study the diversity of fungal communities: The
1227 Glycoside Hydrolase 63 gene. **17,** e11, doi/10.1111/1755-0998.12678.

1228 **Pieterse, C.M. and Van Loon, L.C.** (2004). NPR1: the spider in the web of induced resistance
1229 signaling pathways. Curr. Opin. Plant Biol. **7,** 456-464, doi/10.1016/j.pbi.2004.05.006.

1230 **Pinedo, C., Wang, C., Pradier, J., Dalmais, B., Choquer, M., Le Pêcheur, P., Morgant, G.,**
1231 **Collado, I.G., Cane, D.E., and Viaud, M.** (2008). Sesquiterpene synthase from the botrydial
1232 biosynthetic gene cluster of the phytopathogen Botrytis cinerea. **3,** 791, doi/10.1021/cb800225v.

1233 **Porquier, A., Morgant, G., Moraga, J., Dalmais, B., Luyten, I., Simon, A., Pradier, J.M.,**
1234 **Amselem, J., Collado, I.G., and Viaud, M.** (2016). The botrydial biosynthetic gene cluster of
1235 Botrytis cinerea displays a bipartite genomic structure and is positively regulated by the putative
1236 Zn(II)2Cys6 transcription factor BcBot6. Fungal Genet. Biol. **96,** 33-46,
1237 doi/10.1016/j.fgb.2016.10.003.

1238 **Porquier, A., Moraga, J., Morgant, G., Dalmais, B., Simon, A., Sghyer, H., Collado, I., and**
1239 **Viaud, M.** (2019). Botcinic acid biosynthesis in Botrytis cinerea relies on a subtelomeric gene
1240 cluster surrounded by relics of transposons and is regulated by the Zn2Cys6 transcription factor
1241 BcBoa13(), doi/10.1007/s00294-019-00952-4.

1242 **Poussereau, N., Creton, S., Billon-Grand, G., Rascle, C., and Fevre, M.** (2001). Regulation of
1243 acp1, encoding a non-aspartyl acid protease expressed during pathogenesis of Sclerotinia
1244 sclerotiorum. Microbiology **147,** 717-726, doi/10.1099/00221287-147-3-717.

1245 **Poussereau, N., Gente, S., Rascle, C., Billon-Grand, G., and Fevre, M.** (2001). aspS encoding
1246 an unusual aspartyl protease from Sclerotinia sclerotiorum is expressed during
1247 phytopathogenesis. FEMS Microbiol. Lett. **194,** 27-32, doi/S0378-1097(00)00500-0 [pii].

1248 **R Core Team** (2014). R: A Language and Environment for Statistical Computing(Vienna,
1249 Austria).

1250 **Robinson, M.D. and Smyth, G.K.** (2008). Small-sample estimation of negative binomial
1251 dispersion, with applications to SAGE data. Biostatistics **9,** 321-332,
1252 doi/10.1093/biostatistics/kxm030.

1253 **Robinson, M.D. and Oshlack, A.** (2010). A scaling normalization method for differential
1254 expression analysis of RNA-seq data. Genome Biol. **11,** r25. Epub 2010 Mar 2, doi/10.1186/gb-
1255 2010-11-3-r25.

1256 **Rodrigues, M.L., Godinho, R.M., Zamith-Miranda, D., and Nimrichter, L.** (2015). Traveling
1257 into Outer Space: Unanswered Questions about Fungal Extracellular Vesicles. PLoS Pathog. **11,**
1258 e1005240, doi/10.1371/journal.ppat.1005240.

1259 **Rossi, F.R., Garriz, A., Marina, M., Romero, F.M., Gonzalez, M.E., Collado, I.G., and**
1260 **Pieckenstain, F.L.** (2011). The sesquiterpene botrydial produced by Botrytis cinerea induces the
1261 hypersensitive response on plant tissues and its action is modulated by salicylic acid and
1262 jasmonic acid signaling. Mol. Plant Microbe Interact. **24,** 888-896, doi/10.1094/MPMI-10-10-
1263 0248.

1264 **Rowe, H.C. and Kliebenstein, D.J.** (2007). Elevated genetic variation within virulence-
1265 associated Botrytis cinerea polygalacturonase loci. Mol. Plant Microbe Interact. **20,** 1126-1137,
1266 doi/10.1094/MPMI-20-9-1126.

1267 **Russell V. Lenth** (2016). Least-Squares Means: The R Package lsmeans. **69,** 1-33,
1268 doi/10.18637/jss.v069.i01.

1269 **Samuel, M., Bleackley, M., Anderson, M., and Mathivanan, S.** (2015). Extracellular vesicles
1270 including exosomes in cross kingdom regulation: a viewpoint from plant-fungal interactions.
1271 Front. Plant. Sci. **6,** 766, doi/10.3389/fpls.2015.00766.

1272 **Schumacher, J., Pradier, J.M., Simon, A., Traeger, S., Moraga, J., Collado, I.G., Viaud, M.,**
1273 **and Tudzynski, B.** (2012). Natural variation in the VELVET gene bcvel1 affects virulence and
1274 light-dependent differentiation in Botrytis cinerea. PLoS One **7,** e47840,
1275 doi/10.1371/journal.pone.0047840.

1276 **Schumacher, J., Simon, A., Cohrs, K.C., Traeger, S., Porquier, A., Dalmais, B., Viaud, M.,**
1277 **and Tudzynski, B.** (2015). The VELVET Complex in the Gray Mold Fungus Botrytis cinerea:
1278 Impact of BcLAE1 on Differentiation, Secondary Metabolism, and Virulence. Mol. Plant
1279 Microbe Interact. **28,** 659-674, doi/10.1094/MPMI-12-14-0411-R.

1280 **Shannon, P., Markiel, A., Ozier, O., Baliga, N.S., Wang, J.T., Ramage, D., Amin, N.,**
1281 **Schwikowski, B., and Ideker, T.** (2003). Cytoscape: a software environment for integrated
1282 models of biomolecular interaction networks. Genome Res. **13,** 2498-2504,
1283 doi/10.1101/gr.1239303.

1284 **Sharma, H.C., Pampapathy, G., Dhillon, M.K., and Ridsdill-Smith, J.T.** (2005). Detached
1285 leaf assay to screen for host plant resistance to Helicoverpa armigera. J. Econ. Entomol. **98,** 568-
1286 576, doi/10.1603/0022-0493-98.2.568.

1287 **Siewers, V., Viaud, M., Jimenez-Teja, D., Collado, I.G., Gronover, C.S., Pradier, J.,**
1288 **Tudzynski, B., and Tudzynski, P.** (2005). Functional analysis of the cytochrome P450
1289 monooxygenase gene bcbot1 of Botrytis cinerea indicates that botrydial is a strain-specific
1290 virulence factor. **18,** 602, doi/10.1094/MPMI-18-0602.

1291 **Soltis, N.E., Atwell, S., Shi, G., Fordyce, R., Gwinner, R., Gao, D., Shafi, A., and**
1292 **Kliebenstein, D.** (2018). Crop domestication and pathogen virulence: Interactions of tomato and
1293 *Botrytis* genetic diversity. , doi/10.1101/255992.

1294 **Soltis, N.E., Zhang, W., Corwin, J.A., Atwell, S., and Kliebenstein, D.J.** (2019). Pathogen
1295 genetic control of transcriptome variation in the *Arabidopsis thaliana – Botrytis cinerea*
1296 pathosystem. 577585, doi/10.1101/577585.

1297 **Stefanato, F.L., Abou-Mansour, E., Buchala, A., Kretschmer, M., Mosbach, A., Hahn, M.,**
1298 **Bochet, C.G., Metraux, J.P., and Schoonbeek, H.J.** (2009). The ABC transporter BcatrB from
1299 Botrytis cinerea exports camalexin and is a virulence factor on Arabidopsis thaliana. Plant J. **58,**
1300 499-510, doi/10.1111/j.1365-313X.2009.03794.x.

1301 **Stergiopoulos, I. and de Wit, P.J.** (2009). Fungal effector proteins. Annu. Rev. Phytopathol. **47,**
1302 233-263, doi/10.1146/annurev.phyto.112408.132637.

1303 **Stuart, J.M., Segal, E., Koller, D., and Kim, S.K.** (2003). A gene-coexpression network for
1304 global discovery of conserved genetic modules. Science **302,** 249-255,
1305 doi/10.1126/science.1087447.

1306 **Swierzy, I.J., Handel, U., Kaever, A., Jarek, M., Scharfe, M., Schluter, D., and Luder,**
1307 **C.G.K.** (2017). Divergent co-transcriptomes of different host cells infected with Toxoplasma
1308 gondii reveal cell type-specific host-parasite interactions. Sci. Rep. **7,** w, doi/10.1038/s41598-
1309 017-07838-w.

1310 **Tang, D., Wang, G., and Zhou, J.M.** (2017). Receptor Kinases in Plant-Pathogen Interactions:
1311 More Than Pattern Recognition. Plant Cell **29,** 618-637, doi/10.1105/tpc.16.00891.

1312 **Tayal, P., Raj, S., Sharma, E., Kumar, M., Dayaman, V., Verma, N., Jogawat, A., Dua, M.,**
1313 **Kapoor, R., and Johri, A.K.** (2017). A Botrytis cinerea KLP-7 Kinesin acts as a Virulence
1314 Determinant during Plant Infection. Sci. Rep. **7,** 5, doi/10.1038/s41598-017-09409-5.

1315 **ten Have, A., Dekkers, E., Kay, J., Phylip, L.H., and van Kan, J.A.** (2004). An aspartic
1316 proteinase gene family in the filamentous fungus Botrytis cinerea contains members with novel
1317 features. Microbiology **150,** 2475-2489, doi/10.1099/mic.0.27058-0.

1318 **ten Have, A., Espino, J.J., Dekkers, E., Van Sluyter, S.C., Brito, N., Kay, J., Gonzalez, C.,**
1319 **and van Kan, J.A.** (2010). The Botrytis cinerea aspartic proteinase family. Fungal Genet. Biol.
1320 **47,** 53-65, doi/10.1016/j.fgb.2009.10.008.

1321 **Tien-chye Tan, Daniel Kracher, Rosaria Gandini, Christoph Sygmund, Roman Kittl,**
1322 **Dietmar Haltrich, B Martin Hällberg, Roland Ludwig, and Christina Divne** (2015).

1323 Structural basis for cellobiose dehydrogenase action during oxidative cellulose degradation. **6,**
1324 7542, doi/10.1038/ncomms8542.

1325 **Toruno, T.Y., Stergiopoulos, I., and Coaker, G.** (2016). Plant-Pathogen Effectors: Cellular
1326 Probes Interfering with Plant Defenses in Spatial and Temporal Manners. Annu. Rev.
1327 Phytopathol. **54,** 419-441, doi/10.1146/annurev-phyto-080615-100204.

1328 **Tsuda, K. and Katagiri, F.** (2010). Comparing signaling mechanisms engaged in pattern-
1329 triggered and effector-triggered immunity. Curr. Opin. Plant Biol. **13,** 459-465,
1330 doi/10.1016/j.pbi.2010.04.006.

1331 **Urlacher, V.B. and Girhard, M.** (2012). Cytochrome P450 monooxygenases: an update on
1332 perspectives for synthetic application. Trends Biotechnol. **30,** 26-36,
1333 doi/10.1016/j.tibtech.2011.06.012.

1334 **Van Kan, J.A., Stassen, J.H., Mosbach, A., Van Der Lee, T A, Faino, L., Farmer, A.D.,**
1335 **Papasotiriou, D.G., Zhou, S., Seidl, M.F., Cottam, E., Edel, D., Hahn, M., Schwartz, D.C.,**
1336 **Dietrich, R.A., Widdison, S., and Scalliet, G.** (2017). A gapless genome sequence of the
1337 fungus Botrytis cinerea. Mol. Plant. Pathol. **18,** 75-89, doi/10.1111/mpp.12384.

1338 **Van Vu, B., Itoh, K., Nguyen, Q.B., Tosa, Y., and Nakayashiki, H.** (2012). Cellulases
1339 belonging to glycoside hydrolase families 6 and 7 contribute to the virulence of Magnaporthe
1340 oryzae. Mol. Plant Microbe Interact. **25,** 1135-1141, doi/10.1094/MPMI-02-12-0043-R.

1341 **Venables, W.N. and Ripley, B.D.** (2002). Modern Applied Statistics with S, Fourth Edition ed.
1342 (New York: Springer).

1343 **Walker, A.S., Gladieux, P., Decognet, V., Fermaud, M., Confais, J., Roudet, J., Bardin, M.,**
1344 **Bout, A., Nicot, P.C., Poncet, C., and Fournier, E.** (2015). Population structure and temporal
1345 maintenance of the multihost fungal pathogen Botrytis cinerea: causes and implications for
1346 disease management. Environ. Microbiol. **17,** 1261-1274, doi/10.1111/1462-2920.12563.

1347 **Walz, A., Zingen-Sell, I., Loeffler, M., and Sauer, M.** (2008). Expression of an oxalate oxidase
1348 gene in tomato and severity of disease caused by Botrytis cinerea and Sclerotinia sclerotiorum.
1349 **57,** 453-458, doi/10.1111/j.1365-3059.2007.01815.x.

1350 **Wang, C.M., Hopson, R., Lin, X., and Cane, D.E.** (2009). Biosynthesis of the sesquiterpene
1351 botrydial in Botrytis cinerea. Mechanism and stereochemistry of the enzymatic formation of
1352 presilphiperfolan-8beta-ol. J. Am. Chem. Soc. **131,** 8360-8361, doi/10.1021/ja9021649.

1353 **Weiberg, A., Wang, M., Lin, F.M., Zhao, H., Zhang, Z., Kaloshian, I., Huang, H.D., and**
1354 **Jin, H.** (2013). Fungal small RNAs suppress plant immunity by hijacking host RNA interference
1355 pathways. Science **342,** 118-123, doi/10.1126/science.1239705.

1356 **Westermann, A.J., Barquist, L., and Vogel, J.** (2017). Resolving host-pathogen interactions by
1357 dual RNA-seq. PLoS Pathog. **13,** e1006033, doi/10.1371/journal.ppat.1006033.

1358 **Williamson, B., Tudzynski, B., Tudzynski, P., and van Kan, J.A.** (2007). Botrytis cinerea: the
1359 cause of grey mould disease. Mol. Plant. Pathol. **8,** 561-580, doi/10.1111/j.1364-
1360 3703.2007.00417.x.

1361 **Windram, O., Madhou, P., McHattie, S., Hill, C., Hickman, R., Cooke, E., Jenkins, D.J.,**
1362 **Penfold, C.A., Baxter, L., Breeze, E., Kiddle, S.J., Rhodes, J., Atwell, S., Kliebenstein, D.J.,**

1363 **Kim, Y.S., Stegle, O., Borgwardt, K., Zhang, C., Tabrett, A., Legaie, R., Moore, J.,**
1364 **Finkenstadt, B., Wild, D.L., Mead, A., Rand, D., Beynon, J., Ott, S., Buchanan-Wollaston,**
1365 **V., and Denby, K.J.** (2012). Arabidopsis defense against Botrytis cinerea: chronology and
1366 regulation deciphered by high-resolution temporal transcriptomic analysis. Plant Cell **24,** 3530-
1367 3557, doi/10.1105/tpc.112.102046.

1368 **Xie, D.X., Feys, B.F., James, S., Nieto-Rostro, M., and Turner, J.G.** (1998). COI1: an
1369 Arabidopsis gene required for jasmonate-regulated defense and fertility. Science **280,** 1091-
1370 1094, doi/10.1126/science.280.5366.1091.

1371 **Xu, J., Meng, J., Meng, X., Zhao, Y., Liu, J., Sun, T., Liu, Y., Wang, Q., and Zhang, S.**
1372 (2016). Pathogen-Responsive MPK3 and MPK6 Reprogram the Biosynthesis of Indole
1373 Glucosinolates and Their Derivatives in Arabidopsis Immunity. Plant Cell **28,** 1144-1162,
1374 doi/10.1105/tpc.15.00871.

1375 **Xu, L., Liu, F., Lechner, E., Genschik, P., Crosby, W.L., Ma, H., Peng, W., Huang, D., and**
1376 **Xie, D.** (2002). The SCF(COI1) ubiquitin-ligase complexes are required for jasmonate response
1377 in Arabidopsis. Plant Cell **14,** 1919-1935, doi/10.1105/tpc.003368.

1378 **Zamocky, M., Ludwig, R., Peterbauer, C., Hallberg, B.M., Divne, C., Nicholls, P., and**
1379 **Haltrich, D.** (2006). Cellobiose dehydrogenase--a flavocytochrome from wood-degrading,
1380 phytopathogenic and saprotropic fungi. Curr. Protein Pept. Sci. **7,** 255-280,
1381 doi/10.2174/138920306777452367.

1382 **Zhang, B. and Horvath, S.** (2005). A general framework for weighted gene co-expression
1383 network analysis. Stat. Appl. Genet. Mol. Biol. **4,** 6115.1128. Epub 2005 Aug 12,
1384 doi/10.2202/1544-6115.1128.

1385 **Zhang, W., Kwon, S.T., Chen, F., and Kliebenstein, D.J.** (2016). Isolate Dependency of
1386 Brassica rapa Resistance QTLs to Botrytis cinerea. Front. Plant. Sci. **7,** 161,
1387 doi/10.3389/fpls.2016.00161.

1388 **Zhang, W., Corwin, J.A., Copeland, D., Feusier, J., Eshbaugh, R., Chen, F., Atwell, S., and**
1389 **Kliebenstein, D.J.** (2017). Plastic Transcriptomes Stabilize Immunity to Pathogen Diversity:
1390 The Jasmonic Acid and Salicylic Acid Networks within the Arabidopsis/Botrytis Pathosystem.
1391 Plant Cell **29,** 2727-2752, doi/10.1105/tpc.17.00348.